ORIGINAL ARTICLE

Comprehensive investigation and prediction model for mechanical properties of coconut wood–polylactic acid composites filaments for FDM 3D printing

J. Kananathan[1,2] · M. Samykano[2] · K. Kadirgama[3] · D. Ramasamy[2] · M. M. Rahman[2]

Abstract

Fused deposition modeling (FDM) is a practical 3D printing technology to print thermoplastic and composite materials. The FDM 3D printing process has gained substantial attention due to its capability to produce complex and accurate components. Recently, the wood particles-based filament in 3D printing has become a subject of interest, which is due to their prominent advantages, such as thermal resistivity, corrosion resistivity, biodegradable characteristics, and being environmentally friendly. Therefore, this research study aims to investigate the mechanical properties and statistical prediction model development for coconut wood–polylactic acid (PLA). The experimental investigation was carried out according to the ASTM standards (tensile—ASTM D638 Type 1, compression—ASTM D695, and bending—ASTM D790) at different infill densities (25, 50, and 70%) and five different infill patterns. The obtained results proved that concentric infill pattern accompanied by 75% infill percentage achieved the most outstanding tensile and bending behavior. For compression testing, grid infill pattern accompanied by 75% infill percentage exhibits maximum compression properties. In overall, the octagram spiral infill pattern shows the weakest properties among all the infill patterns. The experimental results were further analyzed using response surface methodology to identify the effectiveness of studied parameters on mechanical properties and to derive a mathematical model. The derived mathematical models related to studied mechanical properties have been proposed to predict the desired mechanical properties with respect to the variation of infill patterns and percentages.

1 Introduction

According to the American Society for Testing and Materials (ASTM) (Rauch et al. 2018), Fused Deposition Modeling (FDM) 3D printing is a procedure of creating three-dimensional (3D) solid objects through the formulation of layers on subsequent layers (Conner et al. 2014; Singh and Chhabra 2017; Wu et al. 2018) from digital models. According to the researchers, 3D printing technology opens up new possibilities for minimizing the supply chain time frames in industry and simplifies the production of complicated frameworks (Ghaffar et al. 2018). Additive manufacturing is used extensively in the automotive sector (DebRoy et al. 2018; Thompson et al. 2016; Zhong et al. 2017), aerospace industry (Gu et al. 2012), manufacturing process, medical sector (DebRoy et al. 2018; Gu et al. 2012; Zhao et al. 2018; Liu et al. 2007; Luo et al. 2014), energy sector, and consumer products (Srivatsan and Sudarshan 2015; Piazza and Alexander 2015; Wong and Hernandez 2012; Petrovic et al. 2011; Yang et al. 2002). Additive manufacturing is subcategorized into six common procedures, including material extrusion (ME), VAT photopolymerization, powder bed fusion (PBF polymers), material jetting (MJ), binder jetting (BJ), and powder bed fusion (PBF metals) (Ryan et al. 2018). FDM falls in the material extrusion processes for 3D printing technology. The FDM process uses thermoplastic filament as a feedstock considering important factors such as melting point and extrusion to form the 3D object (Ippolito et al. 1995; Hopkinson et al. 2006). The thermoplastic filament commonly used in the FDM 3D printing process is acrylonitrile butadiene styrene (ABS) and polylactic acid (PLA).

✉ M. Samykano
mahendran@ump.edu.my

1 Green Kingdom Solutions Sdn. Bhd., Taman Salak Selatan, 57100 Kuala Lumpur, Malaysia

2 College of Engineering, Universiti Malaysia Pahang, 26300 Gambang, Pahang, Malaysia

3 Faculty of Mechanical & Automotive Engineering Technology, Universiti Malaysia Pahang, 26600 Pekan, Pahang, Malaysia

The FDM 3D printing process starts with the design using the 3D CAD modeling software such as Solid works and Inventor (Puigoriol-Forcada et al. 2018). Before the object can be printed, the products' CAD file must be converted to a format that the FDM 3D printer can support. It is usually converted to STL format before transferring it to a FDM 3D printer (Boparai et al. 2016). Figure 1 gives a comprehensive overview of FDM extrusion and the deposition process source.

There are several advantages of using an FDM 3D printer, such as cost efficiency, convenience, and material usage efficiency (Alabdullah 2016; Mireles et al. 2012). FDM 3D printing technology can not only print small models for display purposes (Bertsch et al. 2000) but also functional components or parts such as bio-medical devices (Zein et al. 2002; Sitthi-Amorn et al. 2015; Gu and Li 2002), tissue engineering (Bose et al. 2013; Stevens 2008), aerospace engineering (Chua et al. 2010), and automotive components (Pham and Dimov 2012). However, a major downfall of this FDM technology is the longer print time, poor surface finish, and poor mechanical properties. The downfall was reported to be due to the printing parameters (layer thickness, deposition line width, extrusion temperature, raster angles, printing velocity, and the printing orientation), which significantly affects their behavior (Christensen et al. 2018; Wu et al. 2017).

Wood is a naturally available material, and it is non-toxic, biodegradable, corrosion resistive, and has good thermal

Fig. 1 Schematic diagram of FDM extrusion and the deposition process. (Source: Zein et al. 2002)

stability. The possibility of using wood particles as improved FDM 3D printing filaments has received substantial interest. Coconut wood particles are one type of wood material that can be used to formulate composite filaments. The coconut wood particles are added to the PLA in the powder form and extruded in the filament form. The majority of the wood filaments are water sensitive. However, coconut wood is resistant to water, which is an additional advantage. Therefore, the products are hardly affected by cold and high humidity environments. Coconut wood filaments are also suitable for use in marine applications (Tomlinson and Zimmermann 1966). According to the researchers, the wood-based filaments' mechanical properties rely on the printing orientation due to the fiber anisotropy (Le Duigou et al. 2016). The addition of wood particles into the filament is intended to improve properties (Wang et al. 2017). According to Farah's review study, many researchers nowadays focus on PLA-based nanocomposites and the modified products (Farah et al. 2016). Pires et al. (2020) created a prediction model to investigate the effect of crucial printing variables such as mass, mass fluctuation, printing duration, and porosity on the printed specimen properties. They discovered that the size scale, infill pattern, and print temperature all affect the infill percentage, whereas the size scale, printing speed, and layer height all affect the printing time. Petinakis et al. (2009) studied the PLA wood-flour micro-composites with respect to mechanical properties and proved a 20% enhancement in the studied mechanical properties compared to the raw materials. The improvement is believed to be due to the coupling agent that increases the performance of the matrix particles interface adhesion (Petinakis et al. 2009). A group of researchers (Daver et al. 2018) conducted an experimental process to evaluate the cork PLA composites' mechanical, thermal, and morphological properties with different cork content. Their results show, increasing the cork content will improve the tensile properties of the corkwood composites. The impact strength of the composites was found to decrease initially, but with the increase in cork content, the impact strength increases drastically. However, the elasticity of the composites was found to decrease when the cork content is increased (Daver et al. 2018).

Limitation in the working temperature associated with the FDM 3D printing technique permits the use of materials with low melting temperatures, such as PLA and ABS. However, lack of mechanical strength and critical factors such as thermal/electrical conductivity are considered the main drawbacks to these thermoplastic materials. The above-mentioned problems have attracted researchers' attention to boost the FDM 3D printing technique principle by developing new composite filaments. There is still a lack of critical literature in terms of mechanical properties related to these composite filaments incorporating different filler metal compositions as printing parameters. Hence, to the
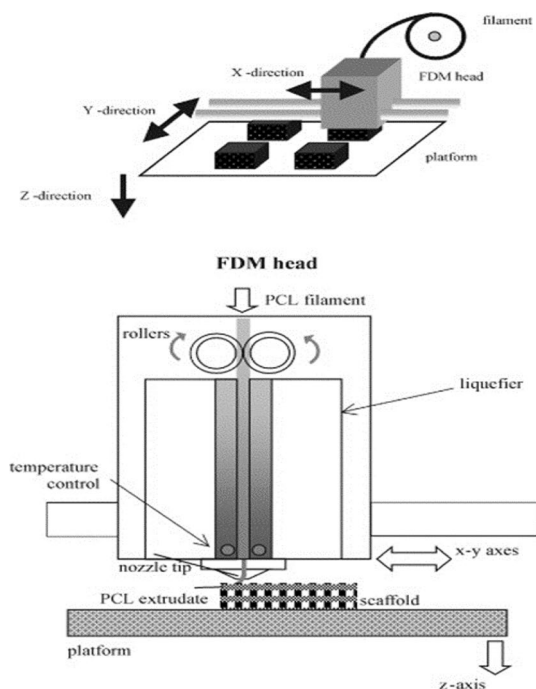
best of the authors' knowledge, this research work reports for the first time the mechanical properties of FDM printed PLA and coconut wood–filled PLA composite as well as a mathematical prediction model for the coconut wood PLA. Critical printing parameters such as infill pattern and infill density with respect to mechanical performance are investigated comprehensively. The response surface methodology is adopted to identify the effective parameters with respect to mechanical properties. Mathematical models are derived using response surface methodology, which predicts desired mechanical properties with respect to the variation of infill patterns and percentages.

2 Materials and methods

2.1 Materials

The material used in this research project, PLA and coconut wood–PLA composite filament, is specially ordered and purchased from Form Futura, Netherlands. The operating temperature of the PLA filament is 180–210 °C, the molecular weight of PLA is 2×10^4 g/mol and the glass transition (T_g) temperature is 55 °C. The coconut wood–PLA filament has 40% coconut wood particles and 60% PLA. A standard 0.5 kg of coconut wood–PLA filament with a diameter of 1.75 mm (± 0.05 mm) is used. The coconut wood–PLA filament characteristics are a wood-like color of the filaments and a processing temperature from 200 to 240 °C.

2.2 Specifications of FDM 3D printer

The FDM 3D printer used for the research project is the WANHAO Duplicator i3 desktop FDM 3D printer. This FDM printer has fulfilled all the minimum requirements needed to print the specimen for mechanical testing. Table 1

shows the specification of the WANHAO Duplicator i3 Desktop FDM 3D printer.

The calibration of the FDM 3D printer is an essential step before starting the printing process. In this research project, calibration has to be done manually for the FDM 3D printer. All three-axis movements (x, y, and z) must be calibrated for a perfect state to print the quality specimen. All the axis must be aligned 180° with respect to the horizontal ground axis. Finally, the alignment of the hotbed is done before the printing process. The distance of the nozzle and the hotbed should be according to the nozzle diameter. A feeler gauge is used to do the calibration. This calibration confirms that the distance between the nozzle and the hotbed is consistent all over the hotbed. Another reason is to ensure that the melted filament is deposited correctly without any oozing or jerking on the printed bed.

2.3 Printing process of the specimen

SolidWorks 2017 edition is used for designing the required specimen. All necessary samples are fabricated according to ASTM standards for the mechanical tests. The designed model is inserted into the slicing software using a flash drive. The software enables a visual g-code to interfere with an STL composer to visualize the STL files on the plate. By using the slicing software, different printing parameters are customized as per the requirements.

The studied parameters are the variation of infill patterns and percentages. G-code generation is the next step after setting all the required parameters. It is a critical factor in maintaining the nozzle's constant temperature and heated bed during the whole printing process. After the printing process ends, the final product is subjected to mechanical testing. All the constant parameters in this research project are summarized in Table 2.
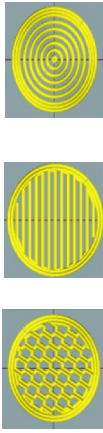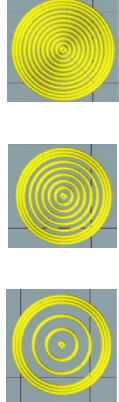
2.4 Parameters and required number of specimens

The chosen parameter values are based on the literature review performed. The values are selected based on high,

Table 1 Specification of WANHAO duplicator i3 desktop FDM 3D printer

Item/properties	Specifications
Extruder	MK10 single-extruder
Print technology	FDM
Build volume	$8 \times 8 \times 7$ in. ($200 \times 200 \times 180$ mm)
Printing speed	10–60 mm/min
Extruder temp	180–240 ℃
Heating plate temp	70–120 ℃
AC input	2A/110 V; 1A/220 V, 50–60 Hz, 250 W
Net weight	10 kg
Overall dimension	$40 \times 41 \times 40$ cm
Firmware	Marlin

Table 2 Constant parameters during the printing process

Parameters	Values (kept constant)
Height of first layer	0.3 mm
Layer height	0.3 mm
Horizontal Shell: solid layer	Top: 1 layer, bottom: 1 layer
Diameter of nozzle	0.4 mm
Diameter of filament	1.75 mm (± 0.05 mm)
Extruder temperature	200 °C (± 2 °C)
Print bed temperature	60 °C (± 2 °C)
Printing speed	30 mm/s

Table 3 Overall specimen to be printed according to the parameters and mechanical test

Printing parameters	Type and number of the test specimen to be printed
Printing pattern	Printing specimen standards (1) Tensile test—(ASTM D638—TYPE 1) (R244) (2) Compression test—(ASTM D695) (3) Bending test—(ASTM D790)
	Number of specimens to be printed
	Printing pattern 5 choices
	Infill density percentage 3 choices

Honeycomb   Rectilinear   Concentric

Octagram Spiral   Grid

Infill density percentages

25%   50%   75%

Therefore, the total number of specimens with a different combination of selected parameters is 15 samples. The sample size of each combination is n=5. Hence, the total number of specimens printed for each mechanical test is 75 specimens. In total, 225 samples are printed for the overall testing process

Table 4 Dimensions of ASTM D638 Type 1 standard specimens

Parameters	Dimensions (mm)
W_c (width of narrow section)	13
L (length of narrow section)	57
W_o (overall width)	19
L_o (overall length)	165
G (gage length)	50
D (distance between grips)	115
R (radius of fillet)	76
T (thickness)	3.2

medium, and low for the infill percentage and different infill patterns such as concentric, grid, honeycomb, octagram spiral, and rectilinear. All the mechanical tests were done for the specimen. Further investigation was conducted to check whether there is a relation between the values of chosen parameters with the printed specimen's mechanical properties. After the first test on the specimen, if there is a relation between the value of the parameter with the mechanical properties, then overall printing was done by varying the value of the parameter as shown in Table 3.

3 Characterization techniques

3.1 Tensile test

The tensile test specimen is designed using the Solid works 2015 and the test is conducted by using INSTRON 3367 machine. The highest capacity that can be exerted by the equipment is 30 kN. For ASTM D368, the recommended speed is 5 mm/min with a tolerance of 25% for the Type 1 specimen geometry. The details of the Type 1 specimen are summarized in Table 4.

3.2 Compression test procedure

Compression test is a test method used to determine the maximum amount of the compressive load on an object before fracturing. During the test, the specimen is placed between the two plates that spread the applied load across the entire surface area of two opposite faces of the printed specimen. A universal test machine will start to push the specimen until it becomes flattened. The compressed specimen is generally shortened with the force's direction and expanded with the direction perpendicular to the force applied. The properties like compressive strength and elastic modulus can all be obtained by conducting this compression test. The results obtained through this compression test

could determine whether the printed specimen is suitable for specific applications, or else it will fail if the applied load exceeds the limit. ASTM D695 is used as a standard reference for compression testing. According to ASTM D695, the testing speed is set at 1.3 ± 0.03 mm/min, and the dimensions of the specimen are in a cylinder shape with 12.7 mm circular diameter and 25.4 mm in length. The compression test specimen is designed using the Solid works 2015 and the testing is performed using INSTRON 3367.

3.3 Bending test

Stiffness and the yield properties of materials are the factors that can be measured through the bending test. Generally, the printed specimens are put on the support span, and the load is exerted to the center by the loading nose to produce a three-point bending. This bending test's main parameters are support span, the loading velocity, and the beam's maximum deflection. The bending test specimens are designed using the Solid works 2015 as per the ASTM D790 standard and the INSTRON 3367 machine was used to conduct this bending test. According to ASTM D790, the specimen's dimensions are 3.2 mm × 12.7 mm × 125 mm.

4 Results and discussion

4.1 Tensile behavior characterization

In the tensile test results, ultimate tensile strength (UTS), elastic modulus (E), and yield strength (0.2% offset) are the main properties investigated. UTS is the highest stress a material could bear before it fails. Elastic modulus, also known as Young's modulus, is mainly used to determine material`s stiffness (Sakurada et al. 1962). Yield strength represents the stress to create a small amount of plastic deformation. The stress–strain curve graph can be plotted based on the generated raw data to find out all the specimen's tensile properties, as shown in Fig. 2. The next step after plotting is to take the average reading of each set of data. Table 5 summarizes the obtained average tensile properties with respect to various infill patterns and percentages.

4.1.1 Ultimate tensile strength (UTS)

The average tensile properties of the PLA and PLA/Coconut wood specimen are shown in Tables 5 and 6. According to Table 5 and Fig. 3, the maximum UTS for the PLA specimen is 37.55 MPa obtained at 75% of infill percentage and concentric infill pattern. The lowest tensile strength of the PLA specimen of 24.80 MPa is obtained at 25% infill percentage and rectilinear infill pattern.

Fig. 2 Stress vs. strain curve of a single specimen with 50% infill percentage and octagram spiral pattern
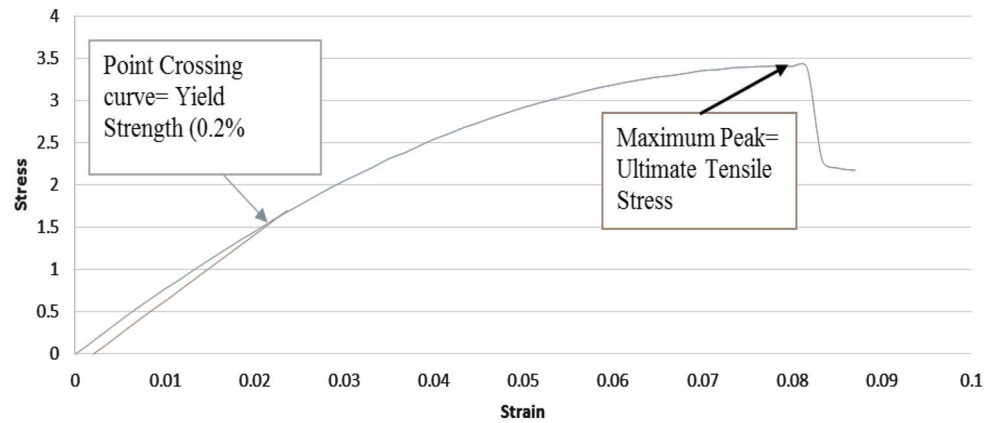
Table 5 Average tensile properties of PLA specimen with various patterns and the infill percentage

Infill pattern	Infill percentage (%)	Young's modulus (GPa)	Tensile strength (Mpa)	Tensile stress at yield (0.2%) (Mpa)
Octagram spiral	25	0.84259	25.42	16.66
Rectilinear	25	0.82934	24.80	16.41
Grid	25	0.83543	25.62	16.59
Honeycomb	25	0.85874	25.33	16.74
Concentric	25	0.86151	25.38	18.36
Octagram spiral	50	0.91949	27.29	18.14
Rectilinear	50	0.86439	26.24	16.69
Grid	50	0.83997	25.98	16.28
Honeycomb	50	0.88192	26.11	17.27
Concentric	50	1.03917	32.66	20.56
Octagram spiral	75	1.02473	30.66	19.99
Rectilinear	75	0.90865	27.78	17.38
Grid	75	0.87069	27.73	17.12
Honeycomb	75	0.92105	27.64	17.74
Concentric	75	1.14776	37.55	23.33

Table 6 Average tensile properties of PLA/Coconut wood specimen with various patterns and the infill percentage

Infill pattern	Infill percentage (%)	Ultimate tensile strength (MPa)	Elastic modulus (GPa)	Yield strength (MPa)
Octagram spiral	25	3.087	0.0747	1.529
Rectilinear	25	3.478	0.0753	1.522
Grid	25	4.202	0.0984	2.261
Honeycomb	25	4.512	0.0932	2.034
Concentric	25	5.358	0.1295	2.872
Octagram Spiral	50	3.488	0.0797	1.755
Rectilinear	50	5.226	0.0888	2.627
Grid	50	5.691	0.1350	3.331
Honeycomb	50	6.449	0.1203	2.840
Concentric	50	9.136	0.1796	4.288
Octagram spiral	75	3.864	0.1078	2.239
Rectilinear	75	7.084	0.1253	3.099
Grid	75	8.351	0.1840	4.609
Honeycomb	75	8.861	0.1832	4.304
Concentric	75	12.185	0.2324	5.959

Referring to Table 6 and Fig. 3, the highest UTS reported belongs to the PLA/Coconut wood specimen with the 75% infill percentage and concentric pattern, 12.185 MPa. The highest value obtained might be attributed to the geometry of the printed specimen as well as better wettability, dispersion, and filler-matrix adhesion due to the well-established interfacial bonding between coconut wood and PLA (Chun et al. 2013). From the results obtained, the UTS was observed to increase as the infill percentage increases. These findings were in accordance with research conducted by Alvarez et al. (2016). Moreover, these results prove that the highest tensile strength belongs to 75% infill percentage followed by 50% and 25%. From the aspect of infill pattern, the specimen with concentric pattern exhibits the UTS strength followed by the

honeycomb, grid, rectilinear, and octagram spiral pattern. Apart from this, the comparison between the pure PLA and PLA/CW composite reveals a significant drop in the composite filament modulus value. The lower modulus value obtained for the composite filament might be contributed by the weak bonding between coconut wood and PLA. The use of a proper or additional bonding agent is suggested to improve the behavior further.

4.1.2 Elastic modulus

Referring to Table 5 and Fig. 4, the maximum elastic modulus of the PLA specimen of 1.147 is found at 75% infill percentage at concentric infill pattern and the lower elastic
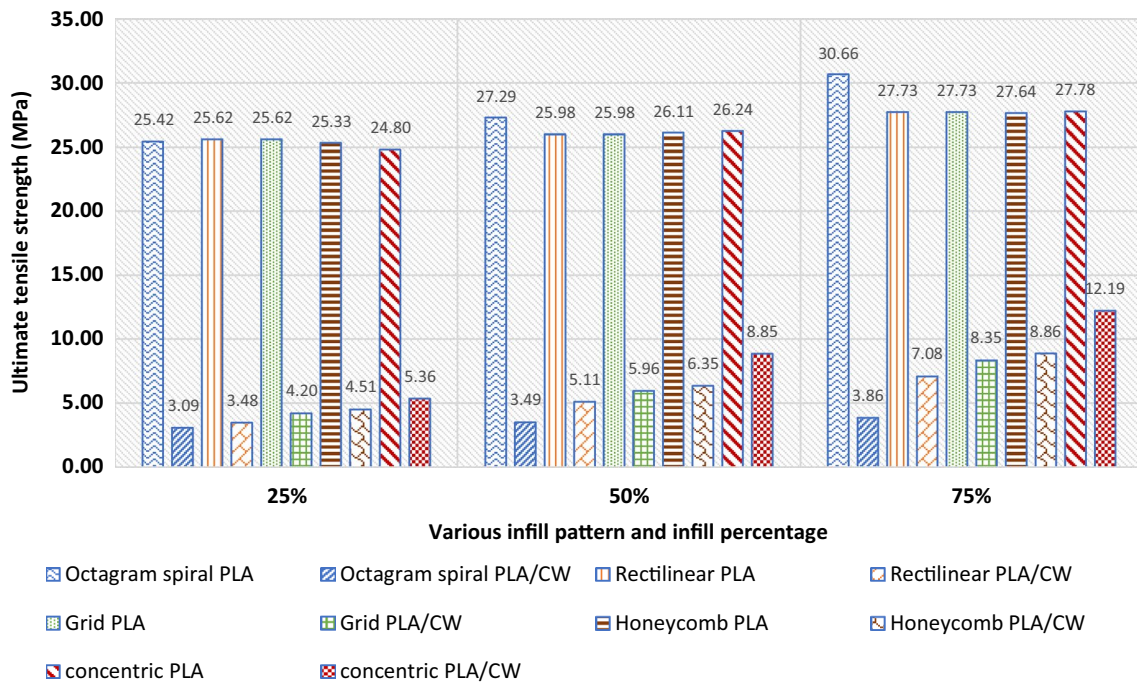
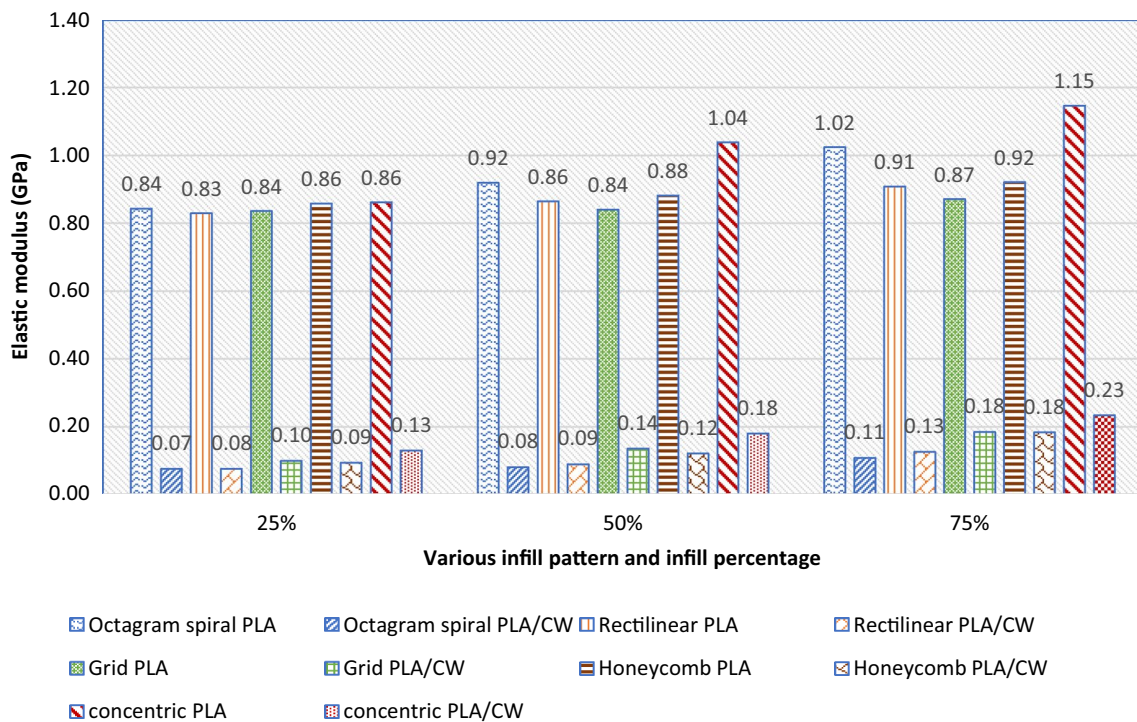**Fig. 3** Bar chart of ultimate tensile strength against infill pattern

Fig. 4 Experimental results of ultimate tensile strength with respect to various infill patterns

modulus of 0.839 at 50% of infill percentage at grid infill pattern. According to Table 6 and Fig. 4, the highest elastic modulus is also associated with PLA/Coconut wood specimen with a 75% infill percentage and concentric infill pattern, contributing 0.2324 GPa. This high elastic modulus is attributed to a higher infill percentage's ability to deform and absorb the stress before a break in the bonds occurs (Fernandez-Vicente et al. 2016). From Fig. 4, it is revealed

that with respect to the variation of infill pattern, if the infill percentage increased, the value of the elastic modulus also increases (Fernandez-Vicente et al. 2016). This is proven with respect to various infill patterns as the highest elastic modulus is achieved by 75% infill percentage followed by 50% and 25%. However, a specimen with a concentric pattern exhibits the highest elastic modulus from infill patterns, followed by the grid, honeycomb, rectilinear, and octagram spiral pattern. Apart from this, the comparison between the pure PLA and PLA/CW composite reveals a significant drop in the composite filament modulus value. The lower modulus value obtained for the composite filament might be contributed by the weak bonding between coconut wood and PLA. The use of a proper or additional bonding agent is suggested to improve the behavior further.
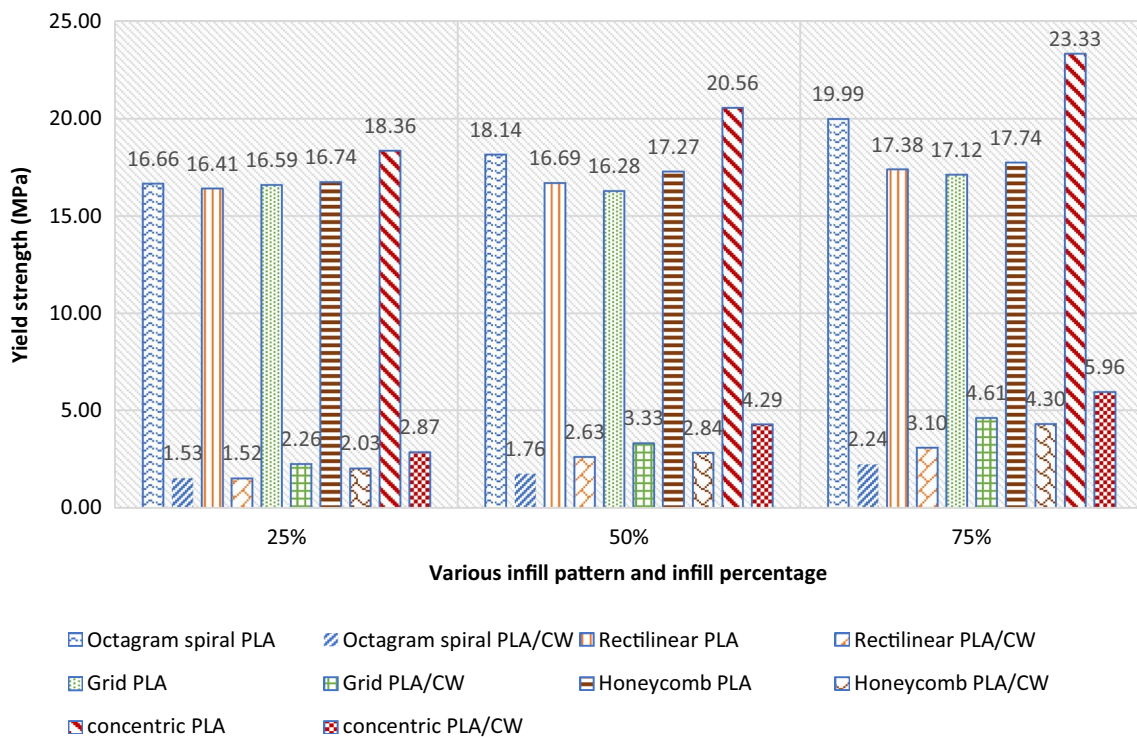
4.1.3 Yield strength (0.2% offset)

The yield properties for the PLA specimen are shown in Table 5 and Fig. 5. The maximum yield strength for the PLA specimen of 23.33 Mpa is achieved at concentric infill pattern at 75% infill percentage. The lowest yield strength of the PLA specimen is recorded at the 50% infill pattern of the grid infill pattern. According to Table 6 and Fig. 5, the highest yield strength (0.2% offset) of PLA/Coconut wood specimen is observed for the specimen with a 75% infill percentage accompanied by a concentric infill pattern

that contributes 5.959 MPa. From Fig. 5, it is obvious that with respect to the variation of infill patterns, if the infill percentage increases, the yield strength (0.2% offset) of the specimen would also increase. This is proven with respect to various infill patterns as the highest yield strength (0.2% offset) is conceded by 75% infill percentage followed by 50% and 25%. However, from the aspect of infill patterns, a specimen with a concentric pattern exhibits the highest yield strength (0.2% offset), followed by the grid, honeycomb, rectilinear, and octagram spiral pattern. Apart from this, the comparison between the pure PLA and PLA/CW composite reveals a significant drop in the composite filament yield strength value. The lower yield strength value obtained for the composite filament might be contributed by the weak bonding between coconut wood and PLA. The use of a proper or additional bonding agent is suggested to improve the behavior further.

4.1.4 Statistical analysis of UTS (PLA/CW filament)

Table 7 states the coefficients 'Coef', standard errors on the estimation of the coefficients 'SE Coef' and P-value. The factors are likely to exhibit a significant effect if the P-value calculated is lower than the alpha value, which is 0.05. If the alpha value exceeds 0.05, it means the factor is not significant and will not affect the mechanical properties (Khuri and Mukhopadhyay 2010). Based on Table 7, infill

**Fig. 5** Bar chart of yield strength (0.2% offset) versus infill pattern

Table 7 ANOVA for UTS (PLA/CW)

Source	DF	Contribution (%)	Adj SS	Adj MS	F-value	P-value
Model	10	99.66	95.0639	9.5064	117.59	0
Linear	5	89.84	85.6995	17.1399	212.01	0
Infill percentage	1	40.72	38.8405	38.8405	480.44	0
Infill pattern	4	49.12	46.859	11.7147	144.91	0
Square	1	0.04	0.0335	0.0335	0.41	0.555
Infill percentage*Infill percentage	1	0.04	0.0335	0.0335	0.41	0.555
2-way interaction	4	9.78	9.3309	2.3327	28.86	0.003
Infill percentage*Infill pattern	4	9.78	9.3309	2.3327	28.86	0.003
Error	4	0.34	0.3234	0.0808		
Total	14	100.00				

$R^2 = 96.35\%$
R^2-adjusted $= 94.32\%$
R^2-predicted $= 89.73\%$

Fig. 6 Pareto chart of UTS (PLA/CW)
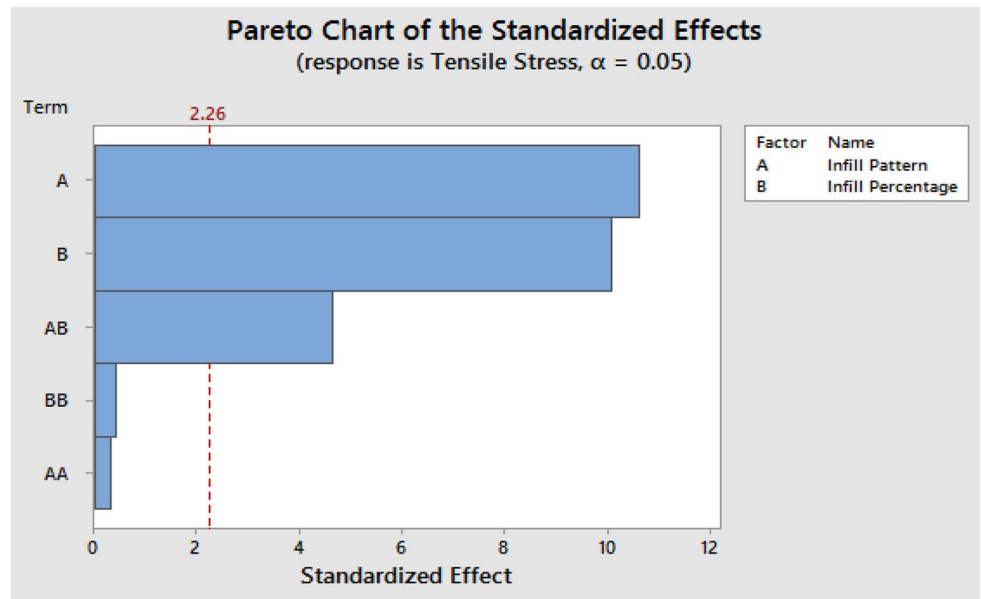
pattern, infill percentage, interaction effect of infill pattern and percentage have a significant effect since their P-value is 0.000, 0.000, and 0.001, respectively, which is less than the alpha value 0.05. Infill patterns contribute almost 49.12%, and infill percentages contribute 40.72%. It shows that both parameters play a significant role in ultimate tensile strength. According to Fig. 6, each bar length is proportional to the absolute value with a 95% confidence level. It is identified that infill pattern, infill percentage, and interaction effect of infill pattern and infill percentage show a compelling impact on the UTS. Table 7 further justifies the statement as two out of the factors mentioned above make the highest contribution to the determination of the UTS of a material. Referring to Table 7, the value of R^2 is equal to 96.35%, indicating that the larger the value of R2, the better the model fits the data.

Moreover, adjusted R^2, which is equal to 94.32%, explains the significance of the relationship. The higher adjusted R^2 indicates that the proposed mathematical model elaborates the relationship between the aspect and response. On the other hand, the model's predictive ability level, known as predicted R^2, is 89.73%. The P-value for the model is 0.000, which is less than the alpha value of 0.05. These results suggest that the model is considered statistically significant. The equation generated through this analysis is shown as Eq. (1). The developed equation is specific for the PLA/CW composite filament properties. Figure 7 shows the residual plot for the ultimate tensile strength. The normal probability shows that almost all the points are near the normal line. This shows the accuracy of the prediction model.
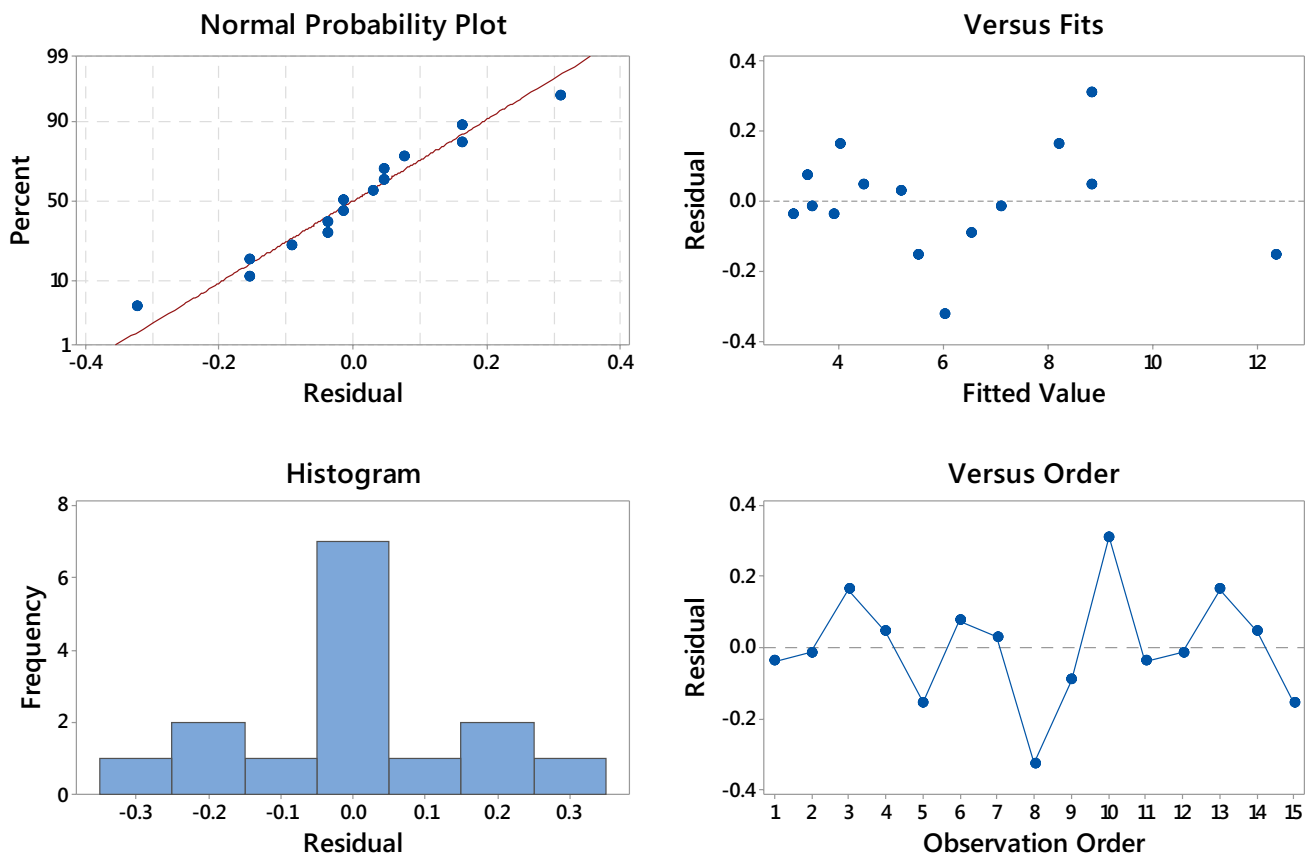
Normal Probability Plot

Versus Fits

Histogram

Versus Order

Fig. 7 Residual plot for UTS (PLA/CW)

$$Ultimate\ Tensile\ Strength\ (PLA/CW) = 3.06 - 0.262\ Infill\ Pattern - 0.0218\ Infill\ Percentage$$
$$+\ 0.0294\ Infill\ Pattern * Infill\ Pattern$$
$$+\ 0.000236\ Infill\ Percentage * Infill\ Percentage \tag{1}$$
$$+\ 0.02568\ Infill\ Pattern * Infill\ Percentage$$

Comparison is also done between the UTS from the experiment and theoretically, and the findings are shown in Table 8 and Fig. 8. Obtained results exhibit negligible average error between the experimental and theoretical values. The calculated error related to the mathematical model for UTS indicates the smallest value of 0.49% and the highest value of 13.09%, with an average value of 5.58%. Therefore, the mathematical model can be highly recommended to estimate the specimen's UTS value.

There was an additional analysis conducted to determine the highest UTS through the response optimization method. This response optimization will help identify the suitable value of the printing parameters used in the given constraint or a certain range to produce the maximum UTS. Based on the investigation, it is observed that the maximum UTS of coconut wood–PLA can reach 11.8088 MPa,

and it can be achieved by the parameter combination of concentric pattern and 75% infill percentage.

4.2 Compressive strength and compressive modulus analysis

In this research work, the compression properties obtained from this testing are compression strength and compression modulus. The compressive stress is obtained by dividing the maximum load from the raw data with the cross-sectional area of a specimen printed (Malhotra 1956). The compression modulus also is the same as the tensile elastic modulus used to determine the stiffness of a material. The determination of the modulus relies on the compressive force. The way to determine the compression strength and compression modulus is the same as the tensile strength and elastic modulus. The stress–strain graph was plotted using the raw

Table 8 Comparison between the experimental and predicted value of UTS

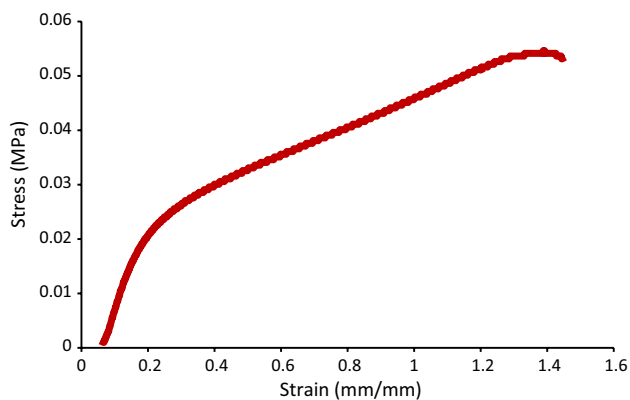| Infill pattern	Infill percentage (%)	Average experimental ultimate tensile strength (MPa)	Predicted ultimate tensile strength (MPa)	Percentage error (%)
Octagram spiral	25	3.087	3.072	0.49
Rectilinear	25	3.478	3.540	1.76
Grid	25	4.202	4.067	3.32
Honeycomb	25	4.512	4.653	3.02
Concentric	25	5.358	5.298	1.15
Octagram spiral	50	3.488	3.611	3.42
Rectilinear	50	5.111	4.722	8.25
Grid	50	5.959	5.891	1.17
Honeycomb	50	6.350	7.118	10.80
Concentric	50	8.846	8.405	5.24
Octagram spiral	75	3.864	4.446	13.09
Rectilinear	75	7.084	6.198	14.29
Grid	75	8.351	8.009	4.27
Honeycomb	75	8.861	9.879	10.30
Concentric	75	12.185	11.808	3.20
				Average = 5.58
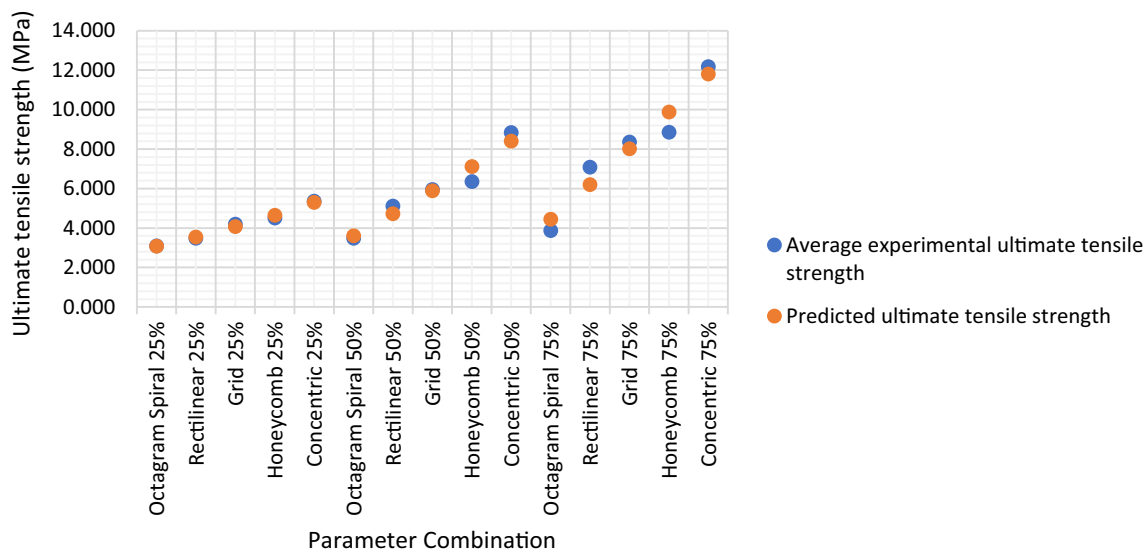
Fig. 8 Comparison of actual and theoretical data of UTS (PLA/CW)

data obtained from the machine software, as shown in Fig. 9. After plotting all the data, the next step is to take the average reading of each set of specimens. Tables 9 and 10 summarize the obtained average compression properties of PLA and PLA/Coconut wood samples regarding various infill patterns and percentages.

4.2.1 Compressive strength

The average compressive properties of the PLA and PLA/Coconut wood specimen are shown in Tables 9 and 10.

According to Table 9 and Fig. 10, the maximum compressive strength obtained at the PLA specimen of 41.22 MPa is found at 75% infill percentage at the grid infill pattern. The lowest compressive strength of the PLA specimen of 23.88 MPa is identified in the 25% infill percentage at rectilinear infill pattern. Referring to Table 10 and Fig. 10, the highest compression strength of the PLA/Coconut wood sample is obtained by the specimen with the 75% infill percentage accompanied by grid pattern, which is 13.738 MPa. The high value obtained might be due to the creation of more surfaces, which could cause

Fig. 9 Stress vs. strain curve with 25% infill percentage and rectilinear infill pattern

Table 9 Average compressive properties of PLA specimen with various patterns and the infill percentage

Infill pattern	Infill percentage (%)	Compression strength (MPa)	Compression modulus (GPa)
Octagram spiral	25	25.638	0.4287
Rectilinear	25	23.883	0.4743
Honeycomb	25	23.973	0.4673
Grid	25	26.187	0.4783
Concentric	25	25.176	0.4199
Octagram spiral	50	31.134	0.6978
Rectilinear	50	28.993	0.5322
Honeycomb	50	30.436	0.6337
Grid	50	36.723	0.8345
Concentric	50	33.876	0.7657
Octagram spiral	75	36.762	0.9365
Rectilinear	75	33.564	0.7834
Honeycomb	75	34.853	0.8342
Grid	75	41.223	1.3198
Concentric	75	39.143	1.3458

Table 10 Average compressive properties of PLA/Coconut wood specimen with various patterns and the infill percentage

Infill pattern	Infill percentage (%)	Compression strength (MPa)	Compression modulus (GPa)
Octagram spiral	25	5.241	0.0786
Rectilinear	25	4.462	0.0600
Honeycomb	25	4.520	0.0609
Grid	25	6.404	0.0915
Concentric	25	5.527	0.0688
Octagram spiral	50	8.969	0.1141
Rectilinear	50	7.356	0.1036
Honeycomb	50	8.147	0.1109
Grid	50	10.417	0.1415
Concentric	50	9.098	0.1307
Octagram spiral	75	12.309	0.1666
Rectilinear	75	12.081	0.1604
Honeycomb	75	12.281	0.1616
Grid	75	13.738	0.1851
Concentric	75	13.239	0.1720

to consume more energy (Li et al. 2007). The results obtained show that the compression strength will be increased with respect to the variation of infill patterns while the infill percentage increases simultaneously. Moreover, these results exhibit that 75% infill percentage has the highest compression strength, followed by the 50% and 25%. From the aspect of various infill patterns, the specimen with the grid pattern exhibits the highest compression strength, followed by the concentric, octagram spiral, honeycomb, and rectilinear pattern. Apart from this, the comparison between the pure PLA and PLA/CW composite reveals a significant drop in the composite filament compressive strength value. The lower compressive strength value obtained for the composite filament might

be contributed by the weak bonding between coconut wood and PLA. The use of a proper or additional bonding agent is suggested to improve the behavior further.

4.2.2 Compressive modulus

According to Table 9 and Fig. 11, the maximum compressive modulus obtained for the PLA specimen of 1.345 GPa is found at 75% infill percentage at the concentric infill pattern. The lowest compressive modulus of the PLA specimen of 0.419 GPa is identified in the 25% infill percentage at the concentric infill pattern. Corresponding to Table 10 and Fig. 11, the highest compression modulus of the PLA/Coconut wood specimen is contributed by 75% infill percentage, and grid infill pattern with 0.185 GPa. This might be due to the inferior cell morphology and large size due to higher infill percentage usage (Vickers 2017). Figure 11 shows that with respect to the variation of infill patterns, as the infill percentage increases, the value of the specimen's compression modulus also increases. This is proven with respect to various infill patterns as the highest compression modulus is achieved by 75% infill percentage followed by 50% and 25%. However, from the aspect of various infill patterns, a specimen with a grid pattern exhibits the highest compression modulus, followed by the concentric, octagram spiral, honeycomb, and rectilinear pattern. Apart from this, the comparison between the pure PLA and PLA/CW composite reveals a significant drop in the composite compressive modulus value. The compressive modulus value obtained for the composite filament might be contributed by the weak bonding between coconut wood and PLA. The
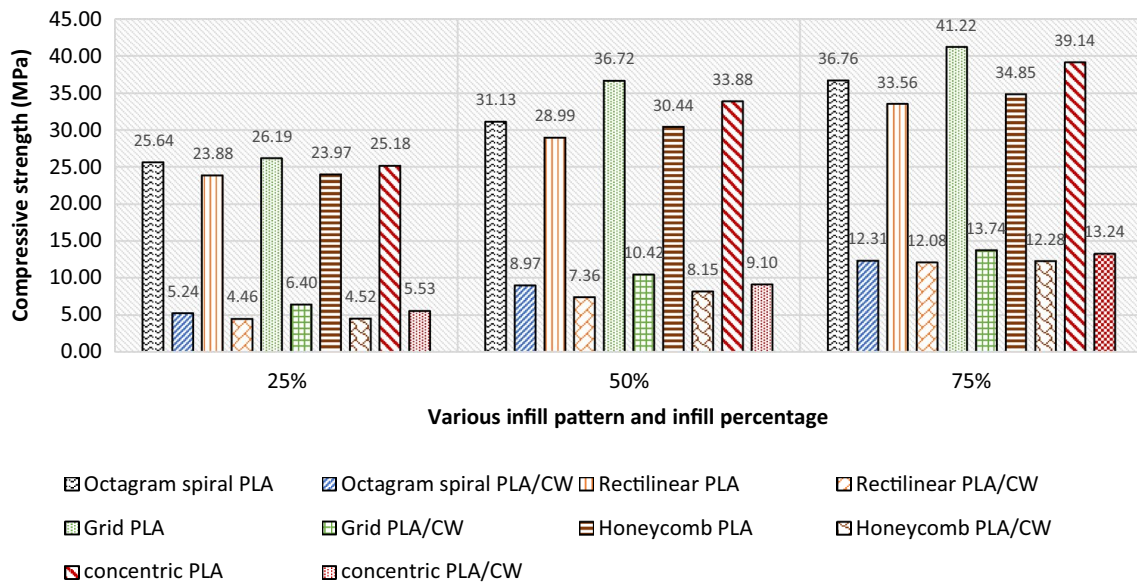
Fig. 10 Experimental results of compressive strength with respect to various infill patterns
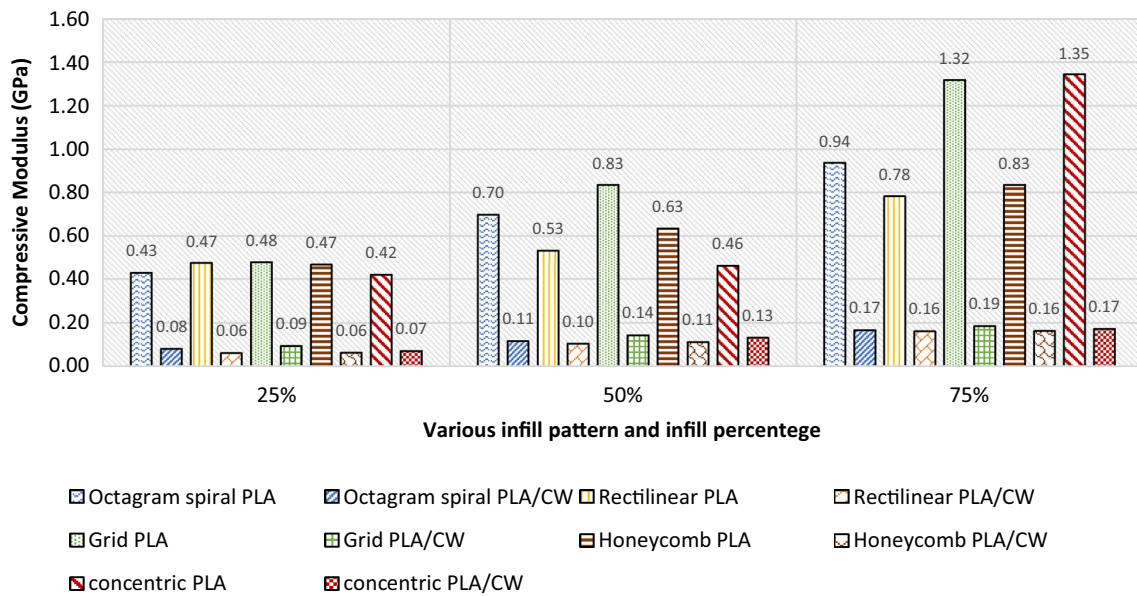

Fig. 11 Experimental results of compressive modulus with respect to various infill patterns

use of a proper or additional bonding agent is suggested to improve the behavior further.

### 4.2.3 Statistical analysis on compression strength (PLA/CW filament)

Based on Table 11, infill patterns contribute almost 6.02%, and infill percentages contribute 93.36%. It shows that only infill percentages have a significant effect on compression strength. The 2-way interaction is insignificant for the

parameters. It shows that the infill pattern has an insignificant effect on the compression strength. Referring to Table 11, the value of R^2 is equal to 99.44%, indicating that the higher the value of R2, the better the model fits the data. The S value equal to 0.30733 suggests that the lower the S value, the better the models predict the response. Moreover, adjusted R^2, which is equal to 99.12%, describes the significance of the relationship. The higher adjusted R^2 indicates that the proposed mathematical model elaborates the relationship between the properties and the response. On the other hand, the model's

Table 11 ANOVA (estimated regression coefficients) for compression strength (PLA/CW)

Source	DF	Contribution (%)	Adj SS	Adj MS	F-value	P-value
Model	10	99.57	149.921	14.992	92.36	0
Linear	5	99.38	149.639	29.928	184.38	0
Infill percentage	1	93.36	140.58	140.58	866.08	0
Infill pattern	4	6.02	9.059	2.265	13.95	0.013
Square	1	0.07	0.111	0.111	0.69	0.454
Infill percentage*Infill percentage	1	0.07	0.111	0.111	0.69	0.454
2-way interaction	4	0.11	0.171	0.043	0.26	0.888
Infill percentage*Infill pattern	4	0.11	0.171	0.043	0.26	0.888
Error	4	0.43	0.649	0.162		
Total	14	100.00				

$R^2 = 99.44\%$
$R^2\text{-adjusted} = 99.12\%$
$R^2\text{-predicted} = 98.08\%$

Fig. 12 Main effect plot (PLA/CW)
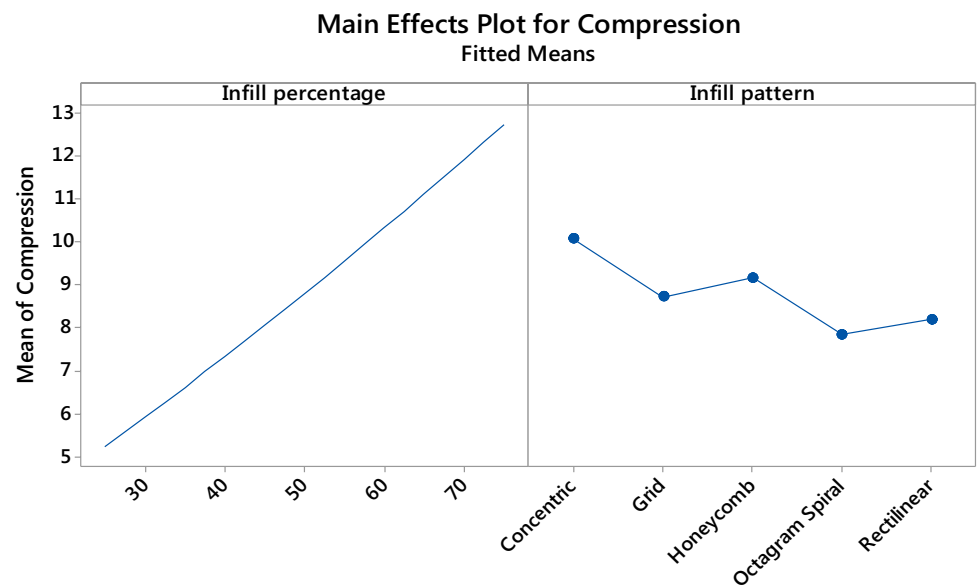
All displayed terms are in the model.

predictive ability level, known as predicted R^2, is 98.08%. The P-value for the model is 0.000, which is less than the alpha value of 0.05. These results suggest that the model is considered statistically significant. The model generated through this analysis is as shown in Eq. (2). As shown in Fig. 12, the mean effect plot indicates that a higher infill percentage produces higher compression strength. The residual plot shows that the points are closer to the normal line, as shown in Fig. 13. This indicates the accuracy of the prediction.

An investigation is done between the obtained compression strength results from the experiment and theoretical approaches, as shown in Table 12 and Fig. 14. The calculated average error between the experimental and theoretical values exhibits a negligible value. The calculated error related to the mathematical model for compression strength ranges from the smallest 0.40% to the largest 6.39%, with the mean value of 2.56%. Therefore, the mathematical model

$$
\begin{aligned}
\text{Compression Strength (PLA/CW Filament)} = {} & 0.732 + 0.165 \text{ Infill Pattern} \\
& + 0.1244 \text{ Infill Percentage} + 0.0730 \text{ Infill Pattern} * \text{Infill Pattern} \\
& + 0.000292 \text{ Infill Percentage} * \text{Infill Percentage} \\
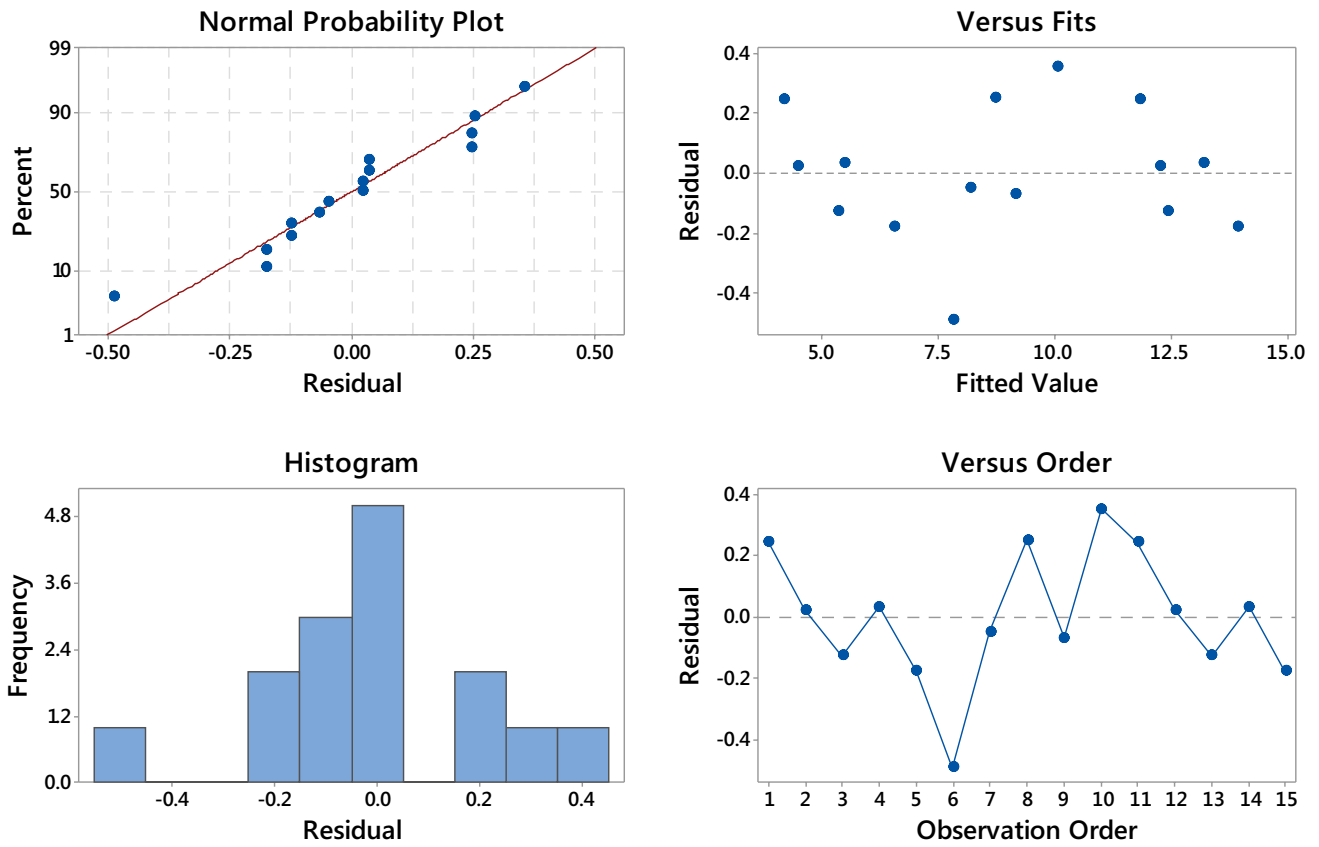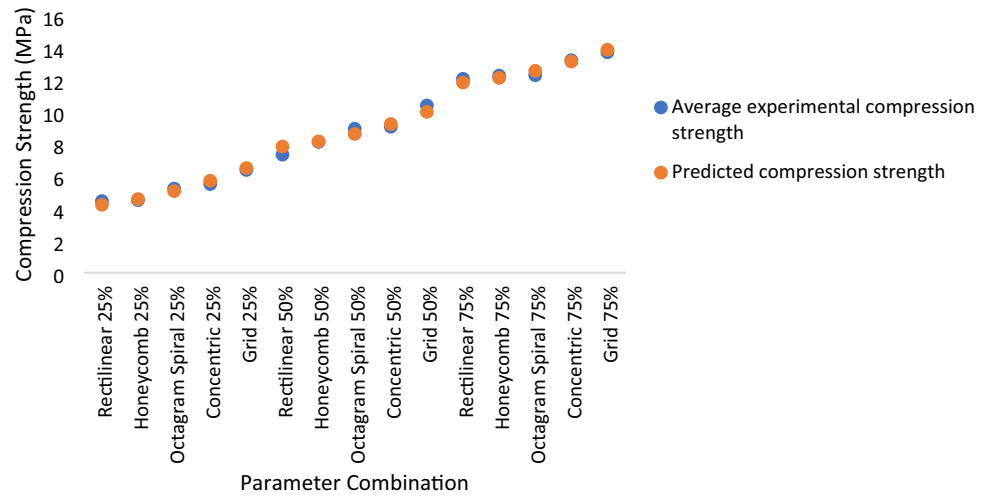& - 0.00124 \text{ Infill Pattern} * \text{Infill Percentage}
\end{aligned}
\tag{2}
$$

Fig. 13 Residual plot for compression strength

Infill pattern	Infill percentage (%)	Average experimental compression strength (MPa)	Predicted compression strength (MPa)	Error (%)
Rectilinear	25	4.462	4.232	5.45
Honeycomb	25	4.520	4.585	1.40
Octagram spiral	25	5.241	5.084	3.10
Concentric	25	5.527	5.729	3.52
Grid	25	6.404	6.520	1.77
Rectilinear	50	7.356	7.858	6.39
Honeycomb	50	8.147	8.180	0.40
Octagram Spiral	50	8.969	8.648	3.72
Concentric	50	9.098	9.262	1.77
Grid	50	10.417	10.022	3.94
Rectilinear	75	12.081	11.850	1.95
Honeycomb	75	12.281	12.141	1.16
Octagram spiral	75	12.309	12.578	2.14
Concentric	75	13.239	13.161	0.60
Grid	75	13.738	13.890	1.09
				Average = 2.56

Table 12 Comparison between the experimental and predicted value of compression strength (PLA/CW)

Fig. 14 Comparison of experimental and predicted data of compression strength (PLA/CW)

can be highly suggested for the prediction or estimation of compression strength.

4.2.4 Statistical analysis on compression modulus (PLA/CW filament)

Based on Table 13, the infill pattern and infill percentage give a significant effect since its P-value is 0.000 and 0.000, respectively, which is less than the alpha value of 0.05. However, the second-order term of infill pattern, infill percentage, and interaction effect of infill pattern and infill percentage does not significantly affect the mechanical properties. According to Fig. 15, where each bar length is proportional to the absolute

modulus. Referring to Table 14, the value of R^2 is equal to 98.97%, indicating that the higher the value of R2, the better the model fits the data. The S value equal to 5.43051 suggests that the models' lower S value predicts the response better. Moreover, adjusted R^2, which is equal to 98.39%, describes the significance of the relationship. The higher adjusted R^2 indicates that the proposed mathematical model elaborates the relationship between the properties and the response. On the other hand, the model's predictive ability level, known as predicted R^2, is 97.62%. The P-value for the model is 0.000, which is less than the alpha value of 0.05. These results suggest that the model is considered statistically significant. The model generated through this analysis is as shown in Eq. (3).

$$
\begin{aligned}
\text{Compression Modulus (PLA/CW Filament)} = {} & 0.0086 + 0.00 \text{ Infill Pattern} \\
& + 0.001951 \text{ Infill Percentage} + 0.001445 \text{ Infill Pattern} * \text{ Infill Pattern} \\
& + 0.00000059 \text{ Infill Percentage} * \text{ Infill Percentage} \\
& - 0.0000224 \text{ Infill Pattern} * \text{ Infill Percentage}
\end{aligned}
\tag{3}
$$

value of the estimated effects with a 95% confidence level, it is identified that infill pattern and infill percentage show a significant impact on the compression modulus. Table 14 proves this statement because two of the factors mentioned above contribute the most to determining a material's compression

Table 13 ANOVA (estimated regression coefficients) for compression modulus (PLA/CW)

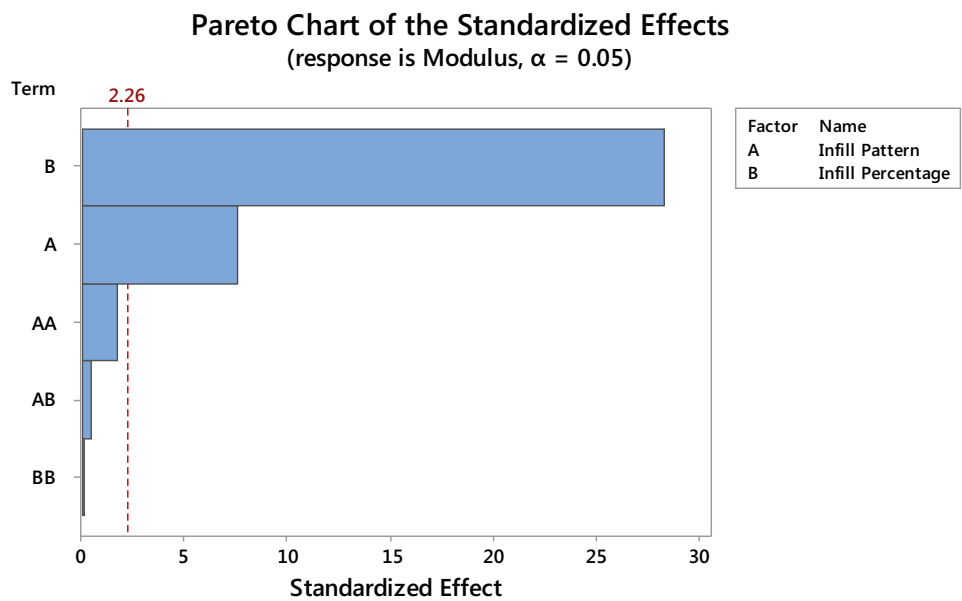| Term	Coef.	SE Coef.	P-value
Constant	117.33	2.95	0.000
Infill pattern	15.10	1.98	0.000
Infill percentage	48.59	1.72	0.000
Infill pattern*Infill pattern	5.78	3.35	0.119
Infill percentage*Infill percentage	0.37	2.97	0.903
Infill pattern*Infill percentage	−1.12	2.43	0.655

An investigation is done between the obtained compression modulus results from the experiment and theoretical approaches, as shown in Table 15 and Fig. 16. From the results obtained, there is a negligible difference between the experimental and theoretical values. The mathematical model error for the compression modulus ranges from the smallest 0.18–13.91%, with a mean value of 3.25%. Therefore, the mathematical model can be highly suggested to predict or estimate the compression modulus.

4.3 Experimental characterization of flexural strength and flexural modulus

In bending tests, the analysis of bending properties included the flexural strength and the flexural modulus. The method to obtain the flexural modulus is the same as the elastic modulus of tensile tests and compression modulus of compression

Fig. 15 Pareto chart of compressive modulus (PLA/CW)

Pareto Chart of the Standardized Effects
(response is Modulus, α = 0.05)

Factor	Name
A	Infill Pattern
B	Infill Percentage

Table 14 ANOVA analysis for compressive modulus (PLA/CW)

Source	DF	Contribution (%)	Adj SS	Adj MS	F-value	P-value
Model	5	98.97	25,412.3	5082.5	172.34	0.000
Linear	2	98.60	25,317.9	12,658.9	429.26	0.000
Infill pattern	1	6.66	1710.0	1710.0	57.98	0.000
Infill percentage	1	91.94	23,607.9	23,607.9	800.53	0.000
Square	2	0.34	88.1	44.1	1.49	0.275
Infill pattern*Infill pattern	1	0.34	87.7	87.7	2.97	0.119
Infill percentage*Infill percentage	1	0.00	0.5	0.5	0.02	0.903
2-way interaction	1	0.02	6.3	6.3	0.21	0.655
Infill pattern*Infill percentage	1	0.02	6.3	6.3	0.21	0.655
Error	9	1.03	265.4	29.5		
Total	14	100.00	25,677.7			

Standard deviation (S) = 5.43051
R^2 = 98.97%
R^2-adjusted = 98.39%
R^2-predicted = 97.62%

tests. The stress–strain curve is plotted from the raw data and used to analyze the properties shown in Fig. 17. Tables 16 and 17 represent the average bending properties between PLA and PLA/Coconut-wood with respect to various infill patterns and percentages.

4.3.1 Flexural strength analysis

The average flexural properties of the PLA and PLA/Coconut wood specimen are shown in Tables 16 and 17. According to Table 16 and Fig. 18, the maximum flexural strength obtained for the PLA specimen of 57.46 MPa is found at 75% of infill percentage at the concentric infill pattern. The lowest compressive strength of the PLA specimen of

42.03 MPa is identified in the 25% infill percentage at rectilinear infill pattern. Referring to Table 17 and Fig. 18, the highest flexural strength is obtained for the PLA/Coconut wood specimen with 75% infill percentage and a concentric pattern of 23.183 MPa. This might be attributed to the higher content of infill percentage (Yap and Teoh 2003). The acquired results show that flexural strength increases with respect to various infill patterns while the infill percentage increases simultaneously. Moreover, these results exhibit that 75% infill percentage has the highest flexural strength, followed by the 50% and 25%. From the aspect of infill patterns, the specimen with concentric pattern exhibits the highest flexural strength followed by the grid, honeycomb, rectilinear, and octagram spiral pattern. Apart

Table 15 Comparison between experimental and predicted value of compression modulus (PLA/CW)

Infill pattern	Infill percentage (%)	Average experimental compression modulus (GPa)	Predicted compression modulus (GPa)	Error (%)
Rectilinear	25	0.0600	0.0586	2.34
Honeycomb	25	0.0609	0.0624	2.39
Octagram spiral	25	0.0786	0.0690	13.91
Concentric	25	0.0688	0.0786	12.38
Grid	25	0.0915	0.0910	0.53
Rectilinear	50	0.1036	0.1079	3.95
Honeycomb	50	0.1109	0.1111	0.18
Octagram spiral	50	0.1141	0.1172	2.66
Concentric	50	0.1307	0.1262	3.53
Grid	50	0.1415	0.1381	2.48
Rectilinear	75	0.1604	0.1580	1.52
Honeycomb	75	0.1616	0.1606	0.62
Octagram spiral	75	0.1666	0.1662	0.28
Concentric	75	0.1720	0.1746	1.51
Grid	75	0.1851	0.1860	0.43
				Average = 3.25

Fig. 16 Comparison of experimental and predicted data of compression modulus (PLA/CW)
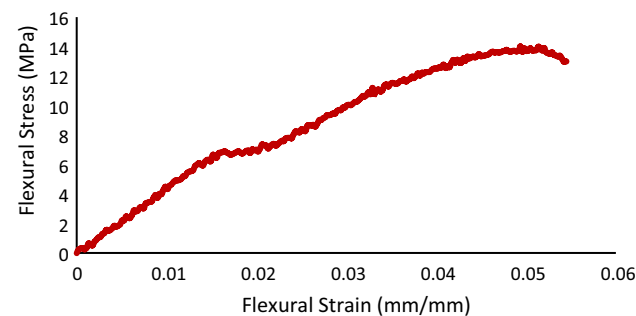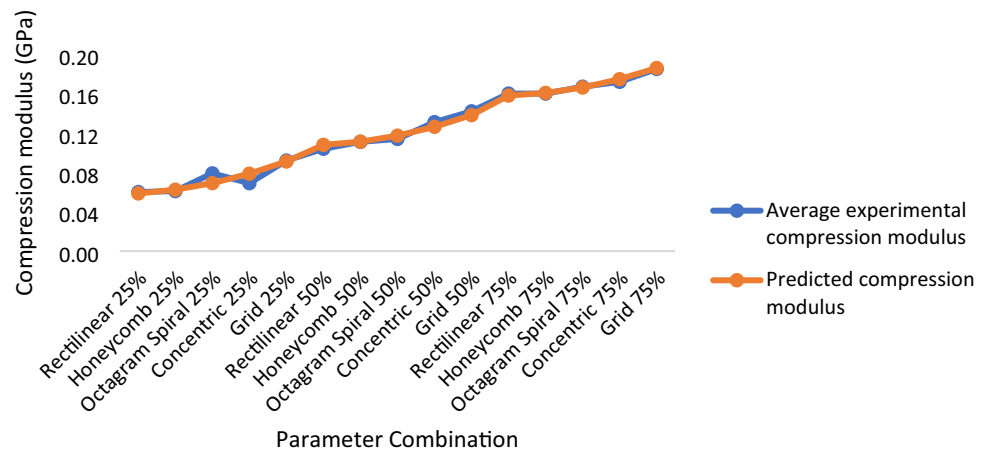
Fig. 17 Flexural stress vs. flexural strain of 75% infill percentage with octagram spiral infill pattern

from this, the comparison between the pure PLA and PLA/CW composite reveals a significant drop in the composite filament flexural strength value. The lower flexural value

obtained for the composite filament might be contributed by the weak bonding between coconut wood and PLA. The use of a proper or additional bonding agent is suggested to improve the behavior further.

4.3.2 Flexural modulus analysis

According to Table 16 and Fig. 19, the maximum flexural modulus obtained for the PLA specimen is 2.94 GPa and was found at 75% infill percentage at concentric infill pattern. The lowest flexural modulus of the PLA specimen is 1.08 GPa, which is identified in a 25% infill percentage at the octagram spiral infill pattern. According to Table 17 and Fig. 19, the highest flexural modulus is related to the specimen with a 75% infill percentage, accompanied by a concentric infill pattern that contributes to a 0.52 GPa. Compared with the PLA/Coconut wood composite specimens, the

Table 16 Average bending properties of PLA specimens of each pattern and the infill percentage

Infill pattern	Infill percentage (%)	Flexural strength (MPa)	Flexural modulus (GPa)
Octagram spiral	25	42.112	1.0793
Rectilinear	25	42.033	1.1110
Honeycomb	25	42.339	1.2974
Grid	25	42.112	1.2378
Concentric	25	45.761	1.3654
Octagram spiral	50	45.654	1.8945
Rectilinear	50	46.774	2.1324
Honeycomb	50	48.387	2.3754
Grid	50	52.832	2.5582
Concentric	50	53.772	2.8112
Octagram spiral	75	50.264	2.4345
Rectilinear	75	53.223	2.7223
Honeycomb	75	54.236	2.6933
Grid	75	55.287	2.7123
Concentric	75	57.457	2.9429

Table 17 Average bending properties of PLA/Coconut wood specimen of each pattern and the infill percentage

Infill pattern	Infill percentage (%)	Flexural strength (MPa)	Flexural modulus (GPa)
Octagram spiral	25	7.137	0.2067
Rectilinear	25	7.500	0.2424
Honeycomb	25	9.070	0.3018
Grid	25	9.937	0.3128
Concentric	25	13.517	0.3586
Octagram spiral	50	11.697	0.3112
Rectilinear	50	12.970	0.3235
Honeycomb	50	13.250	0.3547
Grid	50	16.063	0.3554
Concentric	50	19.187	0.3856
Octagram spiral	75	13.950	0.3801
Rectilinear	75	17.063	0.3996
Honeycomb	75	17.090	0.4173
Grid	75	18.160	0.4277
Concentric	75	23.183	0.5151

PLA has better properties. It can be seen from Fig. 19, with respect to various infill patterns, the value of the flexural

modulus of the specimen increases while the infill percentage increases. This is proven with respect to various infill patterns as the highest flexural modulus is achieved by 75% infill percentage followed by the 50% and 25%. However, from the aspect of infill patterns, a specimen with a concentric pattern exhibits the highest flexural modulus, followed by the grid, honeycomb, rectilinear, and octagram spiral pattern. Apart from this, the comparison between the pure PLA and PLA/CW composite reveals a significant drop in the flexural modulus value of the composite filament. The lower flexural modulus value obtained for the composite filament might be contributed by the weak bonding between coconut wood and PLA. The use of a proper or additional bonding agent is suggested to improve the behavior further.

4.3.3 Statistical analysis on flexural strength (PLA/CW filament)

Based on Table 18, infill pattern, infill percentage, and second-order term of infill pattern have a significant effect since their P-value is 0.000, 0.000, and 0.013, respectively, which is less than the alpha value 0.05. However, the second-order term of infill percentage and interaction effect of infill pattern and infill percentage does not significantly impact the mechanical properties.

According to Fig. 20, where each bar length is proportional to the absolute value of the estimated effects with a 95% confidence level, it is identified that infill pattern, infill percentage, and the second-order term of infill pattern have a significant impact on the flexural strength. Table 19 proves the statement because three of the factors mentioned above have the highest contribution to determining a material's flexural strength. Referring to Table 19, the value of R^2 is equal to 97.80%, indicating that the higher the value of R2, the better the model fits the data. The S value equal to 0.840146 suggests that the models' lower S value predicts the response better. Moreover, adjusted R^2, which is equal to 96.58%, describes the significance of the relationship. The higher adjusted R^2 indicates that the proposed mathematical model elaborates the relationship between the properties and the response. On the other hand, the model's predictive ability level, known as predicted R^2, is 93.75%. The P-value for the model is 0.000, which is less than the alpha value of 0.05. These results suggest that the model is considered statistically significant. The model generated from this analysis is as shown in Eq. (4).

$$\begin{aligned} \text{Flexural Strength (PLA/CW Filament)} = {}& 1.12 - 1.079 \text{ Infill Pattern} \\ & + 0.2986 \text{ Infill Percentage} + 0.401 \text{ Infill Pattern} * \text{Infill Pattern} \\ & - 0.001556 \text{ Infill Percentage} * \text{Infill Percentage} \\ & + 0.00873 \text{ Infill Pattern} * \text{ Infill Percentage} \end{aligned} \tag{4}$$
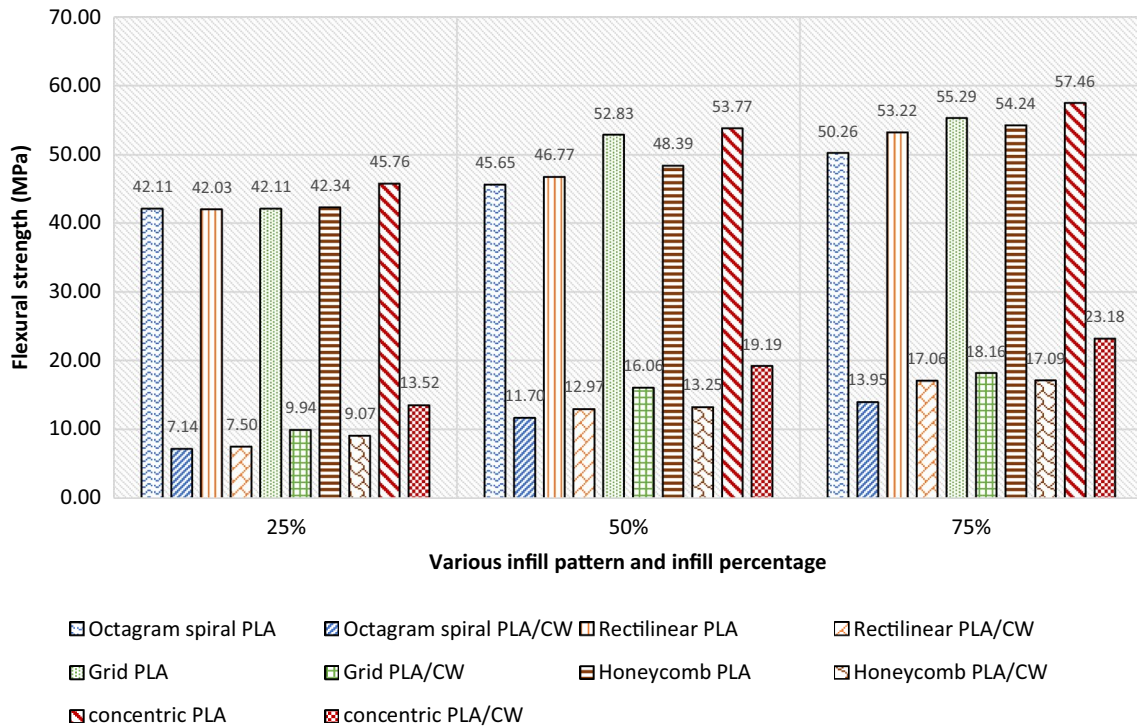
Fig. 18 Experimental results of flexural strength with respect to various infill patterns and infill percentage
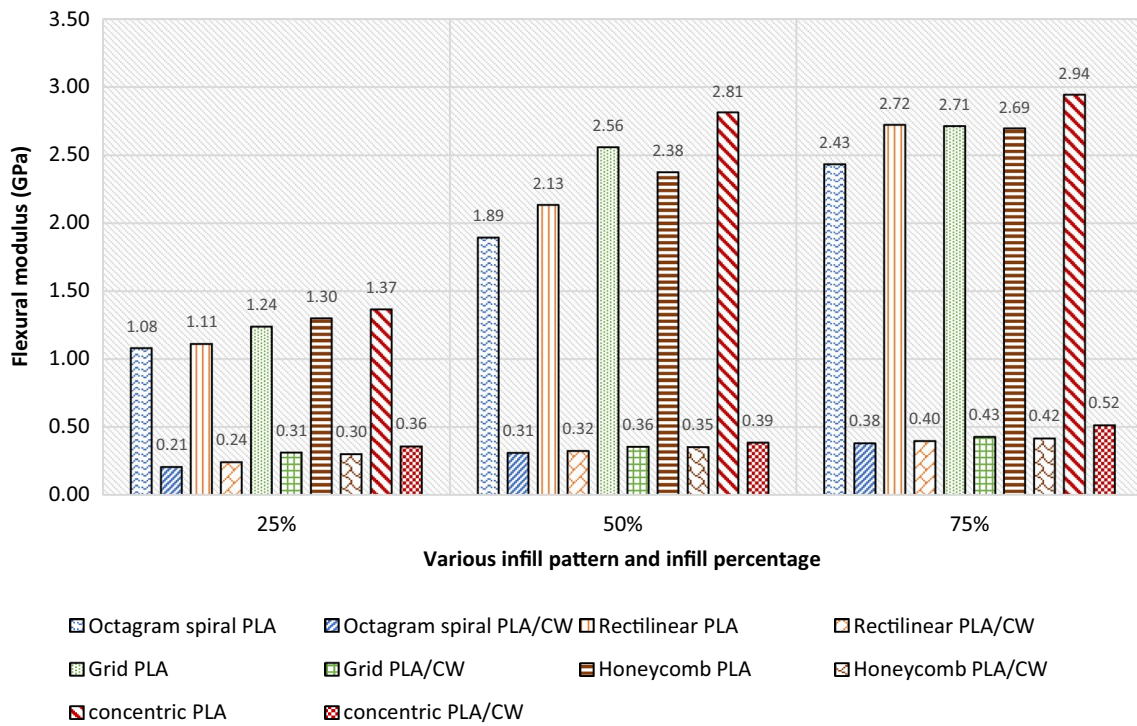

Fig. 19 Experimental results of flexural modulus with respect to various infill patterns and infill percentages

Table 18 ANOVA (estimated regression coefficients) for flexural strength (PLA/CW)

| Term	Coef.	SE Coef.	P-value
Constant	13.832	0.456	0.000
Infill pattern	3.522	0.307	0.000
Infill percentage	4.229	0.266	0.000
Infill pattern*Infill pattern	1.603	0.519	0.013
Infill percentage*Infill percentage	−0.973	0.460	0.064
Infill pattern*Infill percentage	0.437	0.376	0.275

The results of the flexural strength from the experiment and the theoretical approaches are compared in Table 20 and Fig. 21. The calculated error between the experimental and theoretical values exhibits negligible value. The calculated error related to the mathematical model for flexural strength ranges from the smallest 0.05% to the largest 9.96%, with

a mean value of 3.25%. Therefore, the mathematical model can be highly recommended to predict and estimate flexural strength. An additional analysis was also conducted to obtain the possibly highest flexural strength. The response optimization investigation method was used for this purpose. The findings reveal that the maximum flexural strength can reach up to 22.6495 MPa and it can be achieved by the parameter combination of concentric pattern and 75% infill percentage.

4.3.4 Statistical analysis on flexural modulus (PLA/CW filament)

Based on Table 21, infill pattern, infill percentage, and second-order term of infill pattern have a significant effect since their P-value is 0.000, 0.000, and 0.013, respectively, which is less than the alpha value 0.05. However, the second-order term of infill percentage and interaction effect of infill

Fig. 20 Pareto chart of flexural strength (PLA/CW)

Pareto Chart of the Standardized Effects
(response is Flexural Stress, α = 0.05)
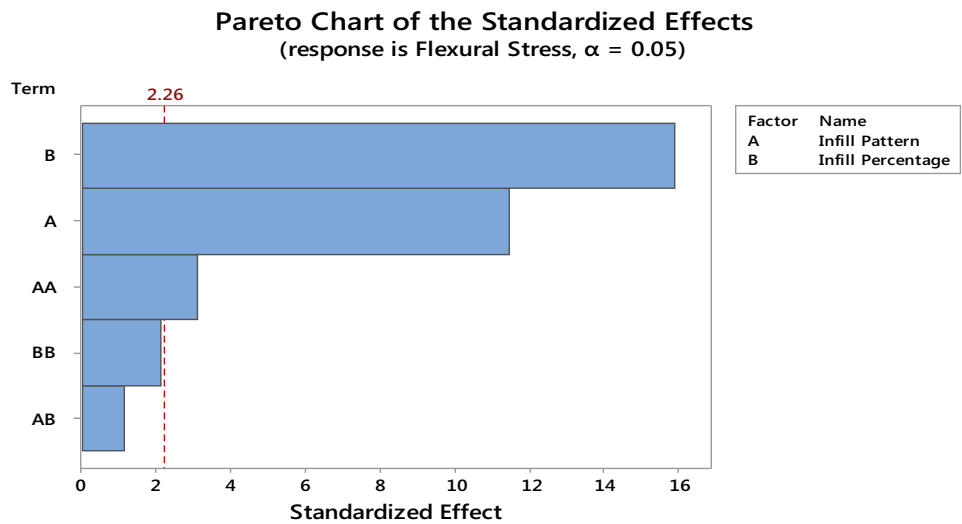
Table 19 ANOVA analysis for flexural strength (PLA/CW)

Source	DF	Contribution (%)	Adj SS	Adj MS	F-value	P-value
Model	5	97.80	282.710	56.542	80.11	0.000
Linear	2	94.05	271.862	135.931	192.58	0.000
Infill pattern	1	32.19	93.045	93.045	131.82	0.000
Infill percentage	1	61.86	178.816	178.816	253.34	0.000
Square	2	3.42	9.895	4.947	7.01	0.015
Infill pattern*Infill pattern	1	2.33	6.741	6.741	9.55	0.013
Infill percentage*Infill percentage	1	1.09	3.154	3.154	4.47	0.064
2-way interaction	1	0.33	0.953	0.953	1.35	0.275
Infill pattern*Infill percentage	1	0.33	0.953	0.953	1.35	0.275
Error	9	2.20	6.353	0.706		
Total	14	100.00	289.063			

Standard deviation (S) = 0.840146
R^2 = 97.80%
R^2-adjusted = 96.58%
R^2-predicted = 93.75%

Table 20 Comparison between the experimental and predicted value of flexural strength (PLA/CW)

Infill pattern	Infill percentage (%)	Average experimental flexural strength (MPa)	Predicted flexural strength (MPa)	Error (%)
Octagram spiral	25	7.137	7.153	0.22
Rectilinear	25	7.500	7.495	0.07
Honeycomb	25	9.070	8.639	4.99
Grid	25	9.937	10.586	6.13
Concentric	25	13.517	13.334	1.37
Octagram spiral	50	11.697	11.919	1.86
Rectilinear	50	12.970	12.479	3.93
Honeycomb	50	13.250	13.842	4.27
Grid	50	16.063	16.006	0.36
Concentric	50	19.187	18.973	1.13
Octagram spiral	75	13.950	14.739	5.35
Rectilinear	75	17.063	15.518	9.96
Honeycomb	75	17.090	17.099	0.05
Grid	75	19.482	19.482	6.78
Concentric	75	23.183	22.666	2.28
				Average = 3.25

Fig. 21 Comparison of experimental and predicted data of flexural strength (PLA/CW)
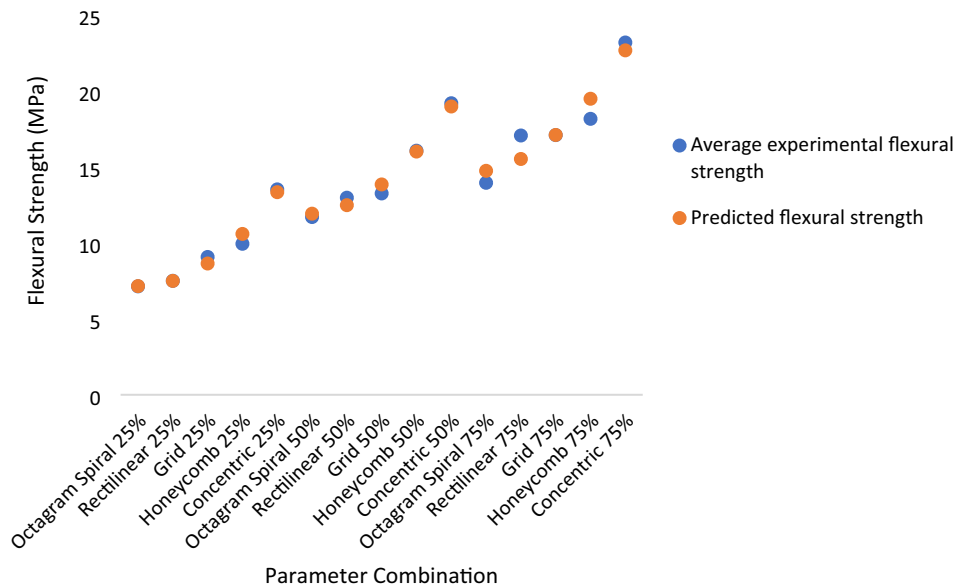
pattern and infill percentage does not significantly affect the mechanical properties.

According to Fig. 22, where each bar length is proportional to the absolute value of the estimated effects with a 95% confidence level, it is identified that infill pattern and infill percentage show a significant impact on the flexural modulus. Table 22 proves the statement because two of the factors mentioned above contribute the most to determining a material's flexural modulus. Referring to Table 22, the value of R^2 is equal to 95.21%, indicating that the higher the value of R2, the better the model fits the data. The S value equal to 20.6941 suggests that the lower the S value, the better the models predict the response. Moreover, adjusted R^2, which is equal to 92.55%, describes the significance of the relationship. The higher adjusted R^2 indicates that the proposed mathematical model elaborates the relationship between the properties and the response. On the other hand, the model's predictive ability level, known as predicted R^2, is 79.95%. The P-value for the model is 0.000, which is less than the alpha value of 0.05. These results suggest that the model is considered statistically significant. The model generated through this analysis is as shown in Eq. (5).

Table 21 ANOVA (estimated regression coefficients) for flexural modulus (PLA/CW)

Term	Coef.	SE Coef.	P-value
Constant	341.1	11.2	0.000
Infill pattern	56.85	7.56	0.000
Infill percentage	71.75	6.54	0.000
Infill pattern*Infill pattern	10.1	12.8	0.452
Infill percentage*Infill percentage	10.1	11.3	0.395
Infill pattern*Infill percentage	−7.58	9.25	0.434

Flexural Modulus (PLA/CW Filament)

$$\begin{aligned} &= 0.1527 + 0.0209 \text{ Infill Pattern} \\ &\quad + 0.00171 \text{ Infill Percentage} \\ &\quad + 0.00251 \text{ Infill Pattern} * \text{Infill Pattern} \\ &\quad + 0.0000162 \text{ Infill Percentage} * \text{Infill Percentage} \\ &\quad - 0.000152 \text{ Infill Pattern} * \text{ Infill Percentage} \end{aligned} \tag{5}$$

The results of the flexural modulus from the experiment and the theoretical approaches are compared in Table 23 and Fig. 23. Based on the result obtained, there is a negligible difference between the experimental and theoretical values. The calculated error related to the mathematical model for flexural modulus ranges from the lowest 0.38% to the highest

Fig. 22 Pareto chart of flexural modulus (PLA/CW)
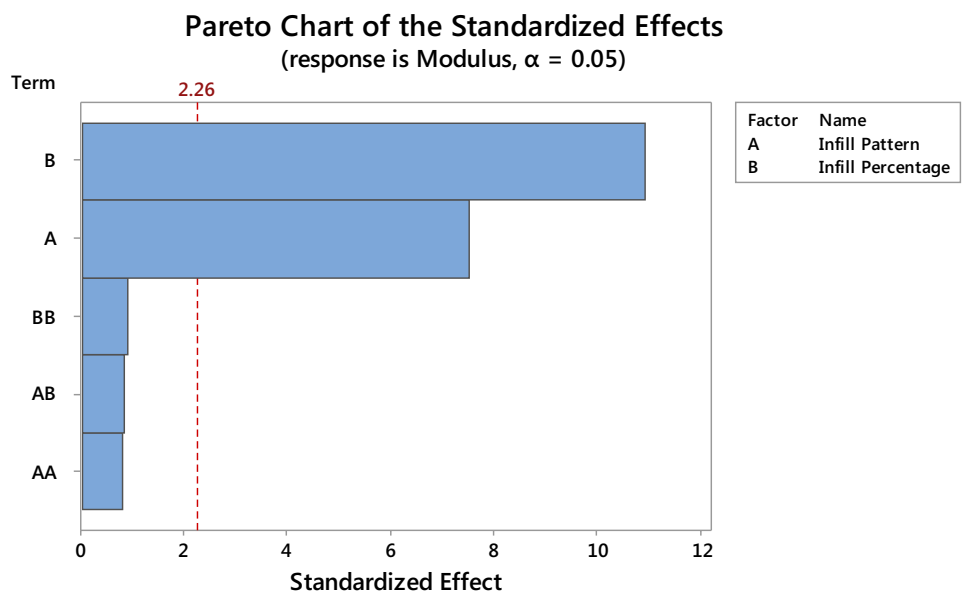
Table 22 ANOVA analysis for flexural modulus (PLA/CW)

| Source	DF	Contribution (%)	Adj SS	Adj MS	F-value	P-value
Model	5	95.21	76,611.9	15,322.4	35.78	0.000
Linear	2	94.10	75,717.9	37,859.0	88.40	0.000
Infill Pattern	1	30.13	24,243.0	24,243.0	56.61	0.000
Infill Percentage	1	63.97	51,474.9	51,474.9	120.20	0.000
Square	2	0.75	606.4	303.2	0.71	0.518
Infill Pattern*Infill Pattern	1	0.33	265.2	265.2	0.62	0.452
Infill Percentage*Infill Percentage	1	0.42	341.1	341.1	0.80	0.395
2-Way Interaction	1	0.36	287.6	287.6	0.67	0.434
Infill Pattern*Infill Percentage	1	0.36	287.6	287.6	0.67	0.434
Error	9	4.79	3854.2	428.2		
Total	14	100.00	80,466.1			

Standard deviation (S) = 20.6941
R^2 = 95.21%
R^2-adjusted = 92.55%
R^2-predicted = 79.95%

Table 23 Comparative test between experimental and predicted value of flexural modulus (PLA/CW)

Infill pattern	Infill percentage (%)	Average experimental flexural modulus (GPa)	Predicted flexural modulus (GPa)	Error (%)
Octagram spiral	25	0.2067	0.2251	8.17
Rectilinear	25	0.2424	0.2498	2.95
Honeycomb	25	0.3018	0.2794	8.00
Grid	25	0.3128	0.3141	0.42
Concentric	25	0.3586	0.3538	1.35
Octagram spiral	50	0.3112	0.2945	5.68
Rectilinear	50	0.3235	0.3153	2.60
Honeycomb	50	0.3547	0.3411	3.97
Grid	50	0.3554	0.3720	4.47
Concentric	50	0.3856	0.4079	5.47
Octagram spiral	75	0.3801	0.3840	1.04
Rectilinear	75	0.3996	0.4011	0.38
Honeycomb	75	0.4173	0.4231	1.38
Grid	75	0.4277	0.4502	4.99
Concentric	75	0.5151	0.4823	6.80
				Average = 3.84

Fig. 23 Pareto chart of flexural modulus (PLA/CW)
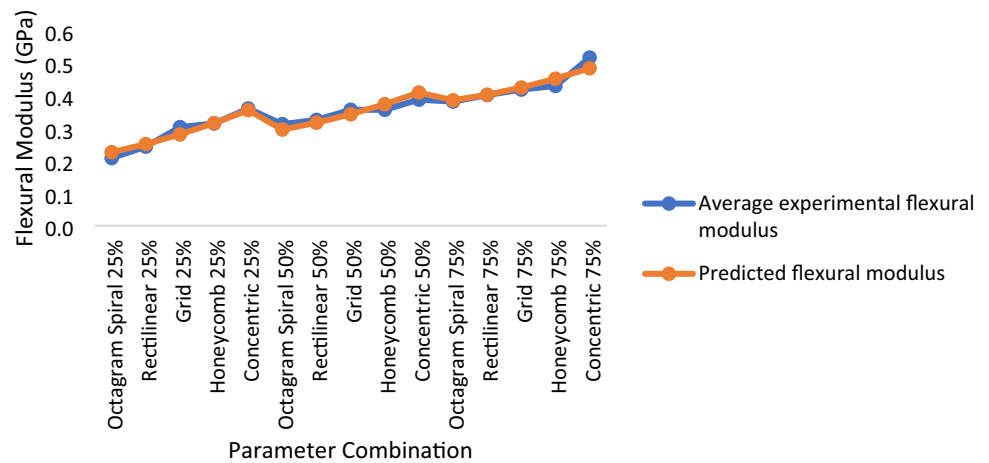
Table 24 Optimized parameters for various strengths of the PLA/Coconut wood specimen

Solution	Infill percentage	Infill pattern	Flexural strength	Compression	UTS	Desirability
1	75	Concentric	23.1378	13.9143	12.3399	0.999059
2	74.9474	Concentric	23.1317	13.9058	12.1858	0.998933
3	74.3904	Concentric	23.0668	13.816	12.1852	0.99758
4	73.9051	Concentric	23.0094	13.738	12.1864	0.996381
5	75	Honeycomb	18.5073	13.2049	12.3399	0.874111
6	75	Honeycomb	18.5073	13.2049	12.1852	0.874111
7	75	Concentric	23.1378	13.9143	8.8152	0.856281
8	73.9057	Concentric	23.0095	13.7381	8.8152	0.853987
9	73.9051	Concentric	23.0094	13.738	8.6854	0.847482
10	73.9051	Concentric	23.0094	13.738	8.5406	0.840113

8.17%, with a mean value of 3.84%. Thus, the mathematical model can be highly recommended for the prediction of flexural modulus. The response optimization results clearly show that the maximum flexural modulus can reach up to 0.4823 GPa. It can be achieved by the parameter combination of concentric pattern and 75% infill percentage.

4.4 Optimization (PLA/CW filament)

The multi-objective optimization was used to find the optimized parameters to get the maximum UTS, compression, and flexural strengths. The closest value to 1 is anticipated to be the best solution for the optimization. The analysis shows that an infill percentage of 75% with an infill pattern of concentric produces the best durability of 0.9990 with UTS of 12.33 MPa, compression strength of 13.91 MPa and flexural strength of 23.13 MPa. Table 24 shows the solution from the analysis.

5 Conclusion

The present work's main purpose is to investigate the PLA and coconut wood–PLA printed mechanical properties using fused deposition modeling. The experimental and statistical evaluation performed elaborates on the effect of the infill pattern, and infill percentage towards the mechanical properties of FDM printed PLA and coconut wood–PLA material. In conclusion, the tensile test results showed that infill pattern, infill percentage, and interaction effect of infill pattern and percentage significantly affect the UTS, elastic modulus, and yield strength (0.2% offset). All the highest tensile properties are achieved by the concentric infill pattern and the 75% infill percentage. The mathematical models generated using RSM for UTS, elastic modulus, and yield strength (0.2% offset) are highly reliable to predict their respective properties since the error occured between the experimental value and the predicted value is below 5.0%. For the second mechanical test, which is compression test, the results show that infill percentage and infill pattern significantly affect both compression strength and compression modulus. All the highest compression properties are achieved by grid infill pattern and 75% infill percentage. Besides, mathematical models generated using RSM for compression strength and compression modulus rely on predicting their respective properties since the error occured between the experimental value and the predicted value is 3.25% for the compression strength and 2.56% for the compression modulus.

For the third mechanical test, which is bending test, the results show that infill percentage and infill pattern have a significant effect on flexural modulus, whereas infill pattern, infill percentage, and second-order term of infill pattern show a significant impact on the flexural strength. All the highest bending properties are achieved by concentric infill pattern and 75% infill percentage. Besides, mathematical models generated using RSM for flexural strength and flexural modulus rely on predicting their respective properties since the error occured between the experimental value and the predicted value is 3.25% for the flexural strength and 3.84% for the flexural modulus.

Another highlight to mention is that the parameter for optimum tensile properties and compression properties is the same: concentric infill pattern and 75% infill percentage. However, the optimum compression properties are grid infill pattern and 75% infill percentage. Thus, infill percentage is essential for all the mechanical properties because a high infill percentage results in a highly packed composition of the product which can withstand a high level of energy on it.

Declarations

Conflict of interest On behalf of all authors, the corresponding author states that there is no conflict of interest.

References

Alabdullah F (2016) Fused deposition modeling (FDM) mechanism. Int J Sci Eng Res 7(5):41–43

Alvarez K, Lagos R, Aizpun M (2016) Investigating the influence of infill percentage on the mechanical properties of fused deposition modelled ABS parts. Inge Investig 36:110–116. https://doi.org/10.15446/ing.investig.v36n3.56610

Bertsch A, Bernhard P, Vogt C, Renaud P (2000) Rapid prototyping of small size objects. Rapid Prototyp J 6(4):259–266

Boparai KS, Singh R, Singh H (2016) Development of rapid tooling using fused deposition modeling: a review. Rapid Prototyp J 22:281–299. https://doi.org/10.1108/RPJ-04-2014-0048

Bose S, Vahabzadeh S, Bandyopadhyay A (2013) Bone tissue engineering using 3D printing. Mater Today 16:496–504

Christensen K, Davis B, Jin Y, Huang Y (2018) Effects of printing-induced interfaces on localized strain within 3D printed hydrogel structures. Mater Sci Eng C 89:65–74. https://doi.org/10.1016/j.msec.2018.03.014

Chua CK, Leong KF, Lim CS (2010) Rapid prototyping: principles and applications (with companion CD-ROM). World Scientific Publishing Company, Singapore

Chun KS, Husseinsyah S, Hakimah O (2013) Properties of coconut shell powder-filled polylactic acid ecocomposites: effect of maleic acid. Polym Eng Sci. https://doi.org/10.1002/pen

Conner BP, Manogharan GP, Martof AN et al (2014) Making sense of 3-D printing: creating a map of additive manufacturing products and services. Addit Manuf 1:64–76. https://doi.org/10.1016/j.addma.2014.08.005

Daver F, Lee KPM, Brandt M, Shanks R (2018) Cork–PLA composite filaments for fused deposition modelling. Compos Sci Technol 168:230–237. https://doi.org/10.1016/j.compscitech.2018.10.008

DebRoy T, Wei HL, Zuback JS et al (2018) Additive manufacturing of metallic components—process, structure and properties. Prog Mater Sci 92:112–224. https://doi.org/10.1016/j.pmatsci.2017.10.001

Farah S, Anderson DG, Langer R (2016) Physical and mechanical properties of PLA, and their functions in widespread applications—a comprehensive review. Adv Drug Deliv Rev 107:367–392. https://doi.org/10.1016/j.addr.2016.06.012

Fernandez-Vicente M, Calle W, Ferrandiz S, Conejero A (2016) Effect of infill parameters on tensile mechanical behavior in desktop 3D printing. 3D Print Addit Manuf 3:183–192. https://doi.org/10.1089/3dp.2015.0036

Ghaffar SH, Corker J, Fan M (2018) Additive manufacturing technology and its implementation in construction as an eco-innovative solution. Autom Constr 93:1–11

Gu P, Li L (2002) Fabrication of biomedical prototypes with locally controlled properties using FDM. CIRP Ann 51:181–184

Gu DD, Meiners W, Wissenbach K, Poprawe R (2012) Laser additive manufacturing of metallic components: materials, processes and mechanisms. Int Mater Rev 57:133–164

Hopkinson N, Hague RJM, Dickens PM (2006) Rapid manufacturing: an industrial revolution for the digital age. Wiley, Chichester

Ippolito R, Iuliano L, Gatto A (1995) Benchmarking of rapid prototyping techniques in terms of dimensional accuracy and surface finish. CIRP Ann 44:157–160

Khuri AI, Mukhopadhyay S (2010) Response surface methodology. Wiley Interdiscip Rev Comput Stat 2:128–149. https://doi.org/10.1002/wics.73

Le Duigou A, Castro M, Bevan R, Martin N (2016) 3D printing of wood fibre biocomposites: from mechanical to actuation functionality. Mater Des 96:106–114

Li S, Song Y, Song Y et al (2007) Carbon foams with high compressive strength derived from mixtures of mesocarbon microbeads and mesophase pitch. Carbon N Y 45:2092–2097. https://doi.org/10.1016/j.carbon.2007.05.014

Liu C, Xia Z, Czernuszka JT (2007) Design and development of three-dimensional scaffolds for tissue engineering. Chem Eng Res Des 85:1051–1064

Luo X, Liu Y, Gu C, Li Z (2014) Study on the progress of solidification, deformation and densification during semi-solid powder rolling. Powder Technol 261:161–169

Malhotra HL (1956) The effect of temperature on the compressive strength of concrete. Mag Concr Res 8:85–94

Mireles J, Espalin D, Roberson D et al (2012) Fused deposition modeling of metals. In: Proceedings of the solid freeform fabrication symposium, Austin, TX, USA, pp 6–8

Petinakis E, Yu L, Edward G et al (2009) Effect of matrix-particle interfacial adhesion on the mechanical properties of poly(lactic acid)/wood-flour micro-composites. J Polym Environ 17:83. https://doi.org/10.1007/s10924-009-0124-0

Petrovic V, Vicente Haro Gonzalez J, Jordá Ferrando O et al (2011) Additive layered manufacturing: sectors of industrial application shown through case studies. Int J Prod Res 49:1061–1079

Pham D, Dimov SS (2012) Rapid manufacturing: the technologies and applications of rapid prototyping and rapid tooling. Springer Science & Business Media, London

Piazza M, Alexander S (2015) Additive manufacturing: a summary of the literature. Urban Publications, Ohio

Pires FQ, Alves-Silva I, Pinho LAG et al (2020) Predictive models of FDM 3D printing using experimental design based on pharmaceutical requirements for tablet production. Int J Pharm 588:119728

Puigoriol-Forcada JM, Alsina A, Salazar-Martín AG et al (2018) Flexural fatigue properties of polycarbonate fused-deposition modelling specimens. Mater Des 155:414–421

Rauch E, Unterhofer M, Dallasega P (2018) Industry sector analysis for the application of additive manufacturing in smart and distributed manufacturing systems. Manuf Lett 15:126–131. https://doi.org/10.1016/j.mfglet.2017.12.011

Ryan J, Dizon C, Espera AH et al (2018) Mechanical characterization of 3D-printed polymers. Addit Manuf 20:44–67

Sakurada I, Nukushina Y, Ito T (1962) Experimental determination of the elastic modulus of crystalline regions in oriented polymers. J Polym Sci 57:651–660

Singh R, Chhabra M (2017) Three-dimensional printing. In: Reference module in materials science and materials engineering. Elsevier, Amsterdam. https://doi.org/10.1016/B978-0-12-803581-8.04167-9

Sitthi-Amorn P, Ramos JE, Wangy Y et al (2015) MultiFab: a machine vision assisted platform for multi-material 3D printing. Acm Trans Graph 34:1–11

Srivatsan TS, Sudarshan TS (2015) Additive manufacturing: innovations, advances, and applications. CRC Press, Boca Raton

Stevens MM (2008) Biomaterials for bone tissue engineering. Mater Today 11:18–25

Thompson MK, Moroni G, Vaneker T et al (2016) Design for additive manufacturing: trends, opportunities, considerations, and constraints. CIRP Ann 65:737–760

Tomlinson P, Zimmermann M (1966) Anatomy of the palm Rhapis excels, III. Juvenile phase. J Arnold Arbor 47:301–312

Vickers NJ (2017) Animal communication: when I'm calling you, will you answer too? Curr Biol 27:R713–R715. https://doi.org/10.1016/j.cub.2017.05.064

Wang X, Jiang M, Zhou Z et al (2017) 3D printing of polymer matrix composites: a review and prospective. Compos Part B Eng 110:442–458. https://doi.org/10.1016/j.compositesb.2016.11.034

Wong KV, Hernandez A (2012) A review of additive manufacturing. ISRN Mech Eng 1:1–10

Wu W, Ye W, Wu Z et al (2017) Influence of layer thickness, raster angle, deformation temperature and recovery temperature on the shape-memory effect of 3D-printed polylactic acid samples. Materials (basel) 10:970

Wu J, Aage N, Westermann R, Sigmund O (2018) Infill optimization for additive manufacturing—approaching bone-like porous structures. IEEE Trans vis Comput Graph 24:1127–1140. https://doi.org/10.1109/TVCG.2017.2655523

Yang S, Dennehy CE, Tsourounis C (2002) Characterizing adverse events reported to the California Poison Control System on herbal remedies and dietary supplements: a pilot study. J Herb Pharmacother 2:1–11

Yap AUJ, Teoh SH (2003) Comparison of flexural properties of composite restoratives using the ISO and mini-flexural tests. J Oral Rehabil 30:171–177. https://doi.org/10.1046/j.1365-2842.2003.01004.x

Zein I, Hutmacher DW, Tan KC, Teoh SH (2002) Fused deposition modeling of novel scaffold architectures for tissue engineering applications. Biomaterials 23:1169–1185

Zhao F, Li D, Jin Z (2018) Preliminary investigation of poly-ether-ether-ketone based on fused deposition modeling for medical applications. Materials (basel) 11:288

Zhong Y, Rännar L-E, Liu L et al (2017) Additive manufacturing of 316L stainless steel by electron beam melting for nuclear fusion applications. J Nucl Mater 486:234–245